

Lyapunov exponents and geodesic stability of Schwarzschild black hole in the non-commutative gauge theory of gravity

Abdellah Touati^{1,*} and Slimane Zaim^{1,‡}

¹*Department of Physics, Faculty of Sciences of Matter, University of Batna-1, Batna 05000, Algeria*

(Dated: February 19, 2025)

In this paper, we study the stability of geodesic motion for both massive and massless particles using Lyapunov exponents in the non-commutative (NC) Schwarzschild black hole (BH) via the gauge theory of gravity. As a first step, we investigate the both time-like and null radial motion of particles, the mean result in NC geometry shows that the particles take infinity proper time to reach the NC singularity (infinite time affine parameter framework for photons). The proper/coordinate time of Lyapunov exponents and their ratio of time-like geodesic for the circular motion of this black hole shows a new behavior, which describes a new range of stable circular orbits between unstable ones. Then we analyze the circular motion of photons, where the result shows a new photon sphere near the event horizon which is not allowed in the commutative case, and the Lyapunov exponent is expressed in this geometry, where this confirms the instability of the outer photon sphere and the stability of the inner one. Moreover, we studied the effect of noncommutativity on the black hole shadow radius, We found a similarity between the non-commutativity and the mass of a black hole. Then we using experimental data from the event horizon telescope, we show that a noncommutativity parameter of the order of $\Theta^{\text{Phy}} \sim 10^{-32}m$.

I. INTRODUCTION

The investigation of geodesic motion for test particles around compact celestial bodies is fundamental in astrophysics, offering valuable insights into the nature of neutron stars, black holes (BHs), and other dense astrophysical objects. The trajectory of particles moving around a BH encodes information about the underlying spacetime geometry, which is shaped by the strong gravitational field of the compact object. This study focuses on analyzing how non-commutative (NC) geometry influences the geodesic motion of test particles near a Schwarzschild BH, employing the Lyapunov exponent [1] as a diagnostic tool. Two key types of geodesic motion often examined in BH physics are radial and circular trajectories. A wide range of studies has previously explored geodesic motion around BHs, such as [2–26]. The classification of stable and unstable orbits sheds light on the spacetime geometry surrounding these objects. The Lyapunov exponent λ provides a means to evaluate the stability of equatorial circular geodesics in BH spacetimes. Depending on the nature of the orbits—whether stable, unstable, or marginally stable—the Lyapunov exponent helps in determining their properties. Circular geodesics in a Schwarzschild BH are integrable, meaning they exhibit no chaotic behavior. In particular, unstable orbits have a positive Lyapunov exponent [1], while stable and marginally stable orbits correspond to imaginary and zero values of the exponent, respectively [1, 27–30]. The importance of geodesic stability has driven numerous studies that utilize Lyapunov exponents to explore various BH spacetimes [31–41].

Recent research has investigated how non-commutativity alters geodesic dynamics using multiple approaches, such as modeling the NC matter distribution through Gaussian functions [42–48] and Lorentzian profiles [49–51], in addition to the star product formalism as well as Bopp’s transformation [52, 53] and NC gauge gravity [54–60]. In previous work [54], we identified a new class of particle motion near the event horizon in an NC spacetime for massive test particles. Here, we extend this analysis to massless particles and other motion types, providing a more comprehensive study of geodesic stability. This work contributes to the ongoing exploration of orbital stability using Lyapunov exponents in NC spacetimes [61–63].

The main objective of this study is to explore the stability of geodesic motion in NC spacetime by analyzing the Lyapunov exponent for different types of particles. We aim to understand how quantum gravity effects, introduced by NC geometry, impact orbital behavior. This investigation enhances our knowledge of stability and chaos in deformed spacetimes, with potential implications for observables such as the innermost stable circular orbit and the BH shadow. NC geometry, which is motivated by string theory [64], is based on the quantization of spacetime, lead-

[†] Corresponding author.

*Electronic address: touati.abph@gmail.com

‡Electronic address: zaim69slimane@yahoo.com

ing to the discretization of gravitational interactions. These quantum gravitational corrections become particularly relevant in the strong-field regions surrounding BHs and should be considered in such analyses.

The coordinate operators in NC spacetime obey the following commutation relation:

$$[x^\mu, x^\nu]_* = i\Theta^{\mu\nu}, \quad (1)$$

where $\Theta^{\mu\nu}$ represents an antisymmetric real matrix that sets the fundamental discretization scale of spacetime. This modification affects the Heisenberg uncertainty principle, leading to a minimum measurable length on the order of the Planck scale:

$$\Delta x^\mu \Delta x^\nu \geq \frac{1}{2} |\Theta^{\mu\nu}|. \quad (2)$$

In the NC framework, the usual function multiplication is replaced by the Moyal star product " $*$ ", which is defined for two functions $f(x)$ and $g(x)$ as follows:

$$(f * g)(x) = f(x) e^{\frac{i}{2} \Theta^{\mu\nu} \overleftarrow{\partial}_\mu \overrightarrow{\partial}_\nu} g(x) \quad (3)$$

$$= f(x)g(x) + \frac{i}{2} \Theta^{\mu\nu} \partial_\mu f(x) \partial_\nu g(x) - \frac{1}{8} \Theta^{\mu\nu} \Theta^{\rho\eta} \partial_\mu \partial_\rho f(x) \partial_\nu \partial_\eta g(x) + \mathcal{O}(\Theta^3). \quad (4)$$

In this study, we adopt the NC gauge gravity approach in conjunction with the Seiberg-Witten (SW) map [64] and star products. NC gauge gravity is a candidate extension of general relativity, maintaining action invariance under NC transformations via the SW map [65–67]. We utilize this framework to derive the NC Schwarzschild metric, then compute the NC corrections to the effective potential and analyze geodesic motion for different particle types. Our findings suggest that both massive and massless particles are prevented from reaching the NC singularity within a finite proper time or affine parameter, while also revealing the presence of novel stable circular orbits near the event horizon—distinct from those predicted in other NC models. Further, we assess the stability of these orbits through Lyapunov exponent analysis, confirming their stability in NC spacetime. Additionally, we determine NC corrections to the BH shadow radius and use observational data to estimate the NC parameter, yielding a fundamental length close to the Planck scale.

The structure of this paper is as follows: Section II details the NC corrections to the metric field using the star product and SW maps. Section III derives the NC geodesic equations and the effective potential, incorporating second-order corrections in Θ . We examine radial and circular motion for both massive and massless particles, studying orbital stability through the Lyapunov exponent. This is followed by an exploration of NC corrections to the BH shadow radius and an estimation of the NC parameter using observational data. The final section summarizes our key results and conclusions.

II. NON-COMMUTATIVE CORRECTIONS FOR SCHWARZSCHILD BLACK HOLE

In this section, we briefly present the NC correction to the Schwarzschild metric within the framework of the gauge theory of gravity. Following the methodology outlined in our previous works [54, 68, 69], we employ both the Seiberg-Witten (SW) map and the star ($*$)-product to construct the NC metric for the Schwarzschild black hole. To obtain the NC gauge potential of gravity, represented by the tetrad fields, we utilize the perturbative expansion of the SW map for the tetrad fields $\hat{e}_\mu^a(x, \Theta)$. This expansion is carried out as a power series in Θ up to second order, as derived in Ref. [70].

$$\begin{aligned} \hat{e}_\mu^a = & e_\mu^a - \frac{i}{4} \Theta^{\nu\rho} [\omega_\nu^{ac} \partial_\rho e_\mu^d + (\partial_\rho \omega_\mu^{ac} + R_{\rho\mu}^{ac}) e_\nu^d] \eta_{cd} + \frac{1}{32} \Theta^{\nu\rho} \Theta^{\lambda\tau} \left[2\{R_{\tau\nu}, R_{\mu\rho}\}^{ab} e_\lambda^c - \omega_\lambda^{ab} (D_\rho R_{\tau\mu}^{cd} + \partial_\rho R_{\tau\mu}^{cd}) e_\nu^m \eta_{dm} \right. \\ & - \{\omega_\nu, (D_\rho R_{\tau\mu} + \partial_\rho R_{\tau\mu})\}^{ab} e_\lambda^c - \partial_\tau \{\omega_\nu, (\partial_\rho \omega_\mu + R_{\rho\mu})\}^{ab} e_\lambda^c - \omega_\lambda^{ab} \left(\omega_\nu^{cd} \partial_\rho e_\mu^m + (\partial_\rho \omega_\mu^{cd} + R_{\rho\mu}^{cd}) e_\nu^m \right) \eta_{dm} \\ & + 2\partial_\nu \omega_\lambda^{ab} \partial_\rho \partial_\tau e_\mu^c - 2\partial_\rho \left(\partial_\tau \omega_\mu^{ab} + R_{\tau\mu}^{ab} \right) \partial_\nu e_\lambda^c - \{\omega_\nu, (\partial_\rho \omega_\lambda + R_{\rho\lambda})\}^{ab} \partial_\tau e_\mu^c - \left(\partial_\tau \omega_\mu^{ab} + R_{\tau\mu}^{ab} \right) \left(\omega_\nu^{cd} \partial_\rho e_\lambda^m \right. \\ & \left. \left. + (\partial_\rho \omega_\lambda^{cd} + R_{\rho\lambda}^{cd}) e_\nu^m \right) \eta_{dm} \right] \eta_{cb}, \end{aligned} \quad (5)$$

and the commutative gauge gravity potentials are denoted by \hat{e}_a^μ and ω_μ^{ab} , which are the tetrad fields and the spin connection, and:

$$\{\alpha, \beta\}^{ab} = (\alpha^{ac} \beta^{db} + \beta^{ac} \alpha^{db}) \eta_{cd}, \quad [\alpha, \beta]^{ab} = (\alpha^{ac} \beta^{db} - \beta^{ac} \alpha^{db}) \eta_{cd} \quad (6)$$

$$D_\mu R_{\rho\sigma}^{ab} = \partial_\mu R_{\rho\sigma}^{ab} + \left(\omega_\mu^{ac} R_{\rho\sigma}^{db} + \omega_\mu^{bc} R_{\rho\sigma}^{da} \right) \eta_{cd}. \quad (7)$$

The component \hat{e}_a^μ is the of the vierbein \hat{e}_μ^a defined as:

$$\hat{e}_\mu^b \hat{e}_a^\mu = \delta_a^b, \quad \hat{e}_\mu^a \hat{e}_a^\nu = \delta_\mu^\nu. \quad (8)$$

In this context, the NC correction to the metric component $\hat{g}_{\mu\nu}$ is obtained according to the following definition [71]:

$$\hat{g}_{\mu\nu} = \frac{1}{2} (\hat{e}_\mu^b * \hat{e}_{\nu b} + \hat{e}_\nu^b * \hat{e}_{\mu b}). \quad (9)$$

In this work we choose the following NC matrix $\Theta^{\mu\nu}$:

$$\Theta^{\mu\nu} = \begin{pmatrix} 0 & 0 & 0 & 0 \\ 0 & 0 & 0 & \Theta \\ 0 & 0 & 0 & 0 \\ 0 & -\Theta & 0 & 0 \end{pmatrix}, \quad \mu, \nu = 0, 1, 2, 3 \quad (10)$$

In order to obtain the NC correction to the metric we follow the same steps in Ref. [54], and we take the same choose of the general tetrads field:

$$\underline{e}_\mu^0 = \left(\left(1 - \frac{2m}{r}\right)^{\frac{1}{2}}, 0, 0, 0 \right), \quad (11a)$$

$$\underline{e}_\mu^1 = \left(0, \left(1 - \frac{2m}{r}\right)^{-\frac{1}{2}} \sin\theta \cos\phi, r \cos\theta \cos\phi, -r \sin\theta \sin\phi \right), \quad (11b)$$

$$\underline{e}_\mu^2 = \left(0, \left(1 - \frac{2m}{r}\right)^{-\frac{1}{2}} \sin\theta \sin\phi, r \cos\theta \sin\phi, r \sin\theta \cos\phi \right), \quad (11c)$$

$$\underline{e}_\mu^3 = \left(0, \left(1 - \frac{2m}{r}\right)^{-\frac{1}{2}} \cos\theta, -r \sin\theta, 0 \right). \quad (11d)$$

The NC tetrads \hat{e}_μ^a are [54]:

$$\hat{e}_0^0 = \left(1 - \frac{2m}{r}\right)^{\frac{1}{2}} + \Theta^2 \left\{ \frac{m \left(88m^2 + mr \left(-77 + 15\sqrt{1 - \frac{2m}{r}} \right) - 8r^2 \left(-2 + \sqrt{1 - \frac{2m}{r}} \right) \right) \sin^2\theta}{32r^5 \left(1 - \frac{2m}{r}\right)^{3/2}} \right\} + \mathcal{O}(\Theta^3) \quad (12a)$$

$$\begin{aligned} \hat{e}_1^1 = & \left(1 - \frac{2m}{r}\right)^{-\frac{1}{2}} \sin\theta \cos\phi - \frac{im\Theta}{4r^2} \left(1 - \frac{2m}{r}\right)^{-\frac{3}{2}} \sin\theta \sin\phi + \Theta^2 \left\{ \frac{m \left(m \left(25 + 2\sqrt{1 - \frac{2m}{r}} \right) r - 2 \left(1 + \sqrt{1 - \frac{2m}{r}} \right) r^2 \right.}{64r^5 \left(1 + \frac{2m}{r}\right)^{5/2}} \right. \\ & \left. + \frac{-24m^2 + \left(24m^2 + m \left(-29 + 6\sqrt{1 - \frac{2m}{r}} \right) \right) r + 2 \left(5 - 3\sqrt{1 - \frac{2m}{r}} \right) r^2}{64r^5 \left(1 + \frac{2m}{r}\right)^{5/2}} \right\} \sin\theta \cos\phi + \mathcal{O}(\Theta^3) \quad (12b) \end{aligned}$$

$$\begin{aligned} \hat{e}_1^2 = & \left(1 - \frac{2m}{r}\right)^{-\frac{1}{2}} \sin\theta \sin\phi + \frac{im\Theta}{4r^2} \left(1 - \frac{2m}{r}\right)^{-\frac{3}{2}} \sin\theta \cos\phi + \Theta^2 \left\{ \frac{m \left(m \left(25 + 2\sqrt{1 - \frac{2m}{r}} \right) r - 2 \left(1 + \sqrt{1 - \frac{2m}{r}} \right) r^2 \right.}{64r^5 \left(1 + \frac{2m}{r}\right)^{5/2}} \right. \\ & \left. + \frac{-24m^2 + \left(24m^2 + m \left(-29 + 6\sqrt{1 - \frac{2m}{r}} \right) \right) r + 2 \left(5 - 3\sqrt{1 - \frac{2m}{r}} \right) r^2}{64r^5 \left(1 + \frac{2m}{r}\right)^{5/2}} \right\} \sin\theta \sin\phi + \mathcal{O}(\Theta^3) \quad (12c) \end{aligned}$$

$$\hat{e}_1^3 = \left(1 - \frac{2m}{r}\right)^{-\frac{1}{2}} \cos\theta + \Theta^2 \left\{ \frac{m \left(-24m^2 + \left(29 - 6\sqrt{1 - \frac{2m}{r}} \right) r - 2 \left(5 - 3\sqrt{1 - \frac{2m}{r}} \right) r^2 \right)}{32r^5 \left(1 + \frac{2m}{r}\right)^{5/2}} \right\} \sin^2\theta \cos\theta + \mathcal{O}(\Theta^3) \quad (12d)$$

$$\begin{aligned} \hat{e}_2^1 = & r \cos \theta \cos \phi + \frac{i\Theta}{4} \left(1 - \left(1 - \frac{2m}{r} \right)^{-\frac{1}{2}} \right) \cos \theta \sin \phi + \Theta^2 \left\{ \frac{m \left(\left(6 - 9\sqrt{1 - \frac{2m}{r}} \right) r + \left(-2 + 5\sqrt{1 - \frac{2m}{r}} \right) r \cos(2\theta) \right. \right. \\ & \left. \left. + \frac{\left(18r + \left(-28 + 8\sqrt{1 - \frac{2m}{r}} \right) m \right) \sin^2 \theta}{64r^3 \left(1 + \frac{2m}{r} \right)^{3/2}} \right\} \cos \theta \cos \phi + \mathcal{O}(\Theta^3) \end{aligned} \quad (12e)$$

$$\begin{aligned} \hat{e}_2^2 = & r \cos \theta \sin \phi - \frac{i\Theta}{4} \left(1 - \left(1 - \frac{2m}{r} \right)^{-\frac{1}{2}} \right) \cos \theta \cos \phi + \Theta^2 \left\{ \frac{m \left(\left(6 - 9\sqrt{1 - \frac{2m}{r}} \right) r + \left(-2 + 5\sqrt{1 - \frac{2m}{r}} \right) r \cos(2\theta) \right. \right. \\ & \left. \left. + \frac{\left(18r + \left(-28 + 8\sqrt{1 - \frac{2m}{r}} \right) m \right) \sin^2 \theta}{64r^3 \left(1 + \frac{2m}{r} \right)^{3/2}} \right\} \cos \theta \sin \phi + \mathcal{O}(\Theta^3) \end{aligned} \quad (12f)$$

$$\begin{aligned} \hat{e}_2^3 = & -r \sin \theta + \Theta^2 \left\{ \frac{m \left(-2m \left(1 + 2\sqrt{1 - \frac{2m}{r}} \right) + \left(m \left(-14 + 4\sqrt{1 - \frac{2m}{r}} \right) + \left(11 - 5\sqrt{1 - \frac{2m}{r}} \right) r \right) \cos(2\theta) \right. \right. \\ & \left. \left. + \frac{r \left(1 + \sqrt{1 - \frac{2m}{r}} \right)}{64r^3 \left(1 + \frac{2m}{r} \right)^{3/2}} \right\} \sin \theta + \mathcal{O}(\Theta^3) \end{aligned} \quad (12g)$$

$$\begin{aligned} \hat{e}_3^1 = & -r \sin \theta \sin \phi + \frac{i\Theta}{4} \left(1 - \left(1 - \frac{2m}{r} \right)^{-\frac{1}{2}} \right) \sin \theta \cos \phi + \Theta^2 \left\{ \frac{m \left(-2r \left(1 - \sqrt{1 - \frac{2m}{r}} \right) + \left(2m \left(9 - 17\sqrt{1 - \frac{2m}{r}} \right) r \right) \right. \right. \\ & \left. \left. + \frac{2r - \left(13 - 17\sqrt{1 - \frac{2m}{r}} \right) r \sin^2 \theta}{32r^3 \left(1 + \frac{2m}{r} \right)^{3/2}} \right\} \sin \theta \sin \phi + \mathcal{O}(\Theta^3) \end{aligned} \quad (12h)$$

$$\begin{aligned} \hat{e}_3^2 = & r \sin \theta \cos \phi + \frac{i\Theta}{4} \left(1 - \left(1 - \frac{2m}{r} \right)^{-\frac{1}{2}} \right) \sin \theta \sin \phi - \Theta^2 \left\{ \frac{m \left(-2r \left(1 - \sqrt{1 - \frac{2m}{r}} \right) + \left(2m \left(9 - 17\sqrt{1 - \frac{2m}{r}} \right) r \right) \right. \right. \\ & \left. \left. + \frac{2r - \left(13 - 17\sqrt{1 - \frac{2m}{r}} \right) r \sin^2 \theta}{32r^3 \left(1 + \frac{2m}{r} \right)^{3/2}} \right\} \sin \theta \cos \phi + \mathcal{O}(\Theta^3). \end{aligned} \quad (12i)$$

Noting that, in the limit of $\Theta = 0$, we recover the commutative tetrad fields (11a-11d).

Using the definition in Eq. (9), along with the above NC tetrad fields, and we stop up to the second order in the NC parameter Θ , one can derive the following nonzero components of the deformed metric $\hat{g}_{\mu\nu}$ in the equatorial plane $\theta = \pi/2$:

$$-\hat{g}_{tt} = \left(1 - \frac{2m}{r} \right) + \left\{ \frac{m \left(88m^2 + mr \left(-77 + 15\sqrt{1 - \frac{2m}{r}} \right) - 8r^2 \left(-2 + \sqrt{1 - \frac{2m}{r}} \right) \right)}{16r^4(-2m+r)} \right\} \Theta^2 + \mathcal{O}(\Theta^4) \quad (13a)$$

$$\hat{g}_{rr} = \left(1 - \frac{2m}{r} \right)^{-1} + \left\{ \frac{m \left(12m^2 + mr \left(-14 + \sqrt{1 - \frac{2m}{r}} \right) - r^2 \left(5 + \sqrt{1 - \frac{2m}{r}} \right) \right)}{8r^2(2m-r)^3} \right\} \Theta^2 + \mathcal{O}(\Theta^4) \quad (13b)$$

$$\hat{g}_{\theta\theta} = r^2 + \left\{ \frac{m \left(m \left(10 - 6\sqrt{1 - \frac{2m}{r}} \right) - \frac{8m^2}{r} + r \left(-3 + 5\sqrt{1 - \frac{2m}{r}} \right) \right)}{16(-2m+r)^2} \right\} \Theta^2 + \mathcal{O}(\Theta^4) \quad (13c)$$

$$\hat{g}_{\phi\phi} = r^2 + \left\{ \frac{5}{8} - \frac{3}{8} \sqrt{1 - \frac{2m}{r}} + \frac{m \left(-17 + \frac{5}{\sqrt{1 - \frac{2m}{r}}} \right)}{16r} + \frac{m^2 \sqrt{1 - \frac{2m}{r}}}{(-2m + r)^2} \right\} \Theta^2 + \mathcal{O}(\Theta^4) \quad (13d)$$

It is evident that, in the limit $\Theta \rightarrow 0$, the commutative Schwarzschild solution is recovered. A detailed discussion of the properties of the obtained metric can be found in Ref. [54] for the equatorial plane, while the general case is discussed in Ref. [69].

As observed, this metric exhibits two distinct surfaces, corresponding to the static limit surface and the event horizon, respectively. These surfaces are determined by solving the following equations:

$$\hat{g}_{00} = 0, \quad 1/\hat{g}_{rr} = 0. \quad (14)$$

The solution to this equations give us respectively the NC static limit surface and the event horizon of the NC Schwarzschild BH [54, 69]:

$$r_{sls}^{NC} = r_h \left[1 + \left(\frac{\Theta}{r_h} \right) \left(\frac{4\sqrt{5} + 1}{32\sqrt{5}} \right) + \left(\frac{\Theta}{r_h} \right)^2 \left(\frac{10 + \sqrt{5}}{128} \right) \right], \quad (15)$$

and

$$r_h^{NC} = r_h \left[1 + \frac{3}{8} \left(\frac{\Theta}{r_h} \right)^2 \right]. \quad (16)$$

It is clear that in the limit of $\Theta = 0$, we recover the commutative event horizon $r_h = 2m$.

III. GEODETIC MOTION AND ITS STABILITY AROUND A NON-COMMUTATIVE SCHWARZSCHILD BLACK HOLE

In this section, we analyze the stability of circular orbits constrained to the equatorial plane (i.e., $\theta = \pi/2$) within the framework of the NC Schwarzschild spacetime. The corresponding spacetime metric is given by:

$$d\hat{s}^2 = \hat{g}_{tt}(r, \Theta) c^2 dt^2 + \hat{g}_{rr}(r, \Theta) dr^2 + \hat{g}_{\phi\phi}(r, \Theta) d\phi^2. \quad (17)$$

The motion of a test particle in the NC spacetime is governed by the Lagrangian:

$$2\mathcal{L} = \hat{g}_{tt}(r, \Theta) c^2 \dot{t}^2 + \hat{g}_{rr}(r, \Theta) \dot{r}^2 + \hat{g}_{\phi\phi}(r, \Theta) \dot{\phi}^2, \quad (18)$$

where the dot denotes differentiation with respect to the affine parameter τ .

Applying the Euler-Lagrange equations, the generalized momenta are obtained as:

$$p_t = c^2 \hat{g}_{tt}(r, \Theta) \dot{t} = E = \text{constant}, \quad (19a)$$

$$p_\phi = \hat{g}_{\phi\phi}(r, \Theta) \dot{\phi} = l = \text{constant}, \quad (19b)$$

$$p_r = \hat{g}_{rr}(r, \Theta) \dot{r}. \quad (19c)$$

Since the Lagrangian is independent of t and ϕ , energy ($p_t = E$) and angular momentum ($p_\phi = l$) are conserved quantities. Consequently, the expressions for \dot{t} and $\dot{\phi}$ become:

$$\dot{t} = \frac{E}{c^2 \hat{g}_{tt}(r, \Theta)}, \quad \dot{\phi} = \frac{l}{\hat{g}_{\phi\phi}(r, \Theta)}. \quad (20)$$

Substituting these relations into the spacetime invariant equation $\hat{g}_{\mu\nu} U^\mu U^\nu \equiv -h$ (where $U^\mu = c^{-1} \frac{dx^\mu}{d\tau}$ is the four-velocity), we obtain the radial equation:

$$\dot{r}^2 = -\frac{E^2}{c^2 \hat{g}_{tt}(r, \Theta) \hat{g}_{rr}(r, \Theta)} - \frac{1}{\hat{g}_{rr}(r, \Theta)} \left(\frac{l^2}{\hat{g}_{\phi\phi}(r, \Theta)} + hc^2 \right), \quad (21)$$

where $h = 1$ for massive particles and $h = 0$ for massless particles.

By incorporating the specific metric components, the radial equation simplifies to:

$$\dot{r}^2 + V_{\text{eff}}(r, \Theta) = 0, \quad (22)$$

where the effective potential $V_{\text{eff}}(r, \Theta)$ for a test particle in NC spacetime up to second order in the NC parameter Θ , is given by:

$$\begin{aligned} V_{\text{eff}}(r, \Theta) = & \left(1 - \frac{2m}{r}\right) \left(\frac{l^2}{r^2} + hc^2\right) - \frac{E^2}{c^2} + \Theta^2 \left\{ -\frac{l^2}{r^4} \left(1 - \frac{2m}{r}\right) \left(\frac{5}{8} - \frac{3}{8}\sqrt{1 - \frac{2m}{r}} + \frac{m\left(-17 + \frac{5}{\sqrt{1 - \frac{2m}{r}}}\right)}{16r}\right) \right. \\ & + \frac{m^2\sqrt{1 - \frac{2m}{r}}}{(-2m + r)^2} \left. + \frac{E^2}{c^2} \left(\frac{m(64m^2 + m(-49 + 13\sqrt{1 - \frac{2m}{r}})r + 2(13 - 3\sqrt{1 - \frac{2m}{r}})r^2)}{16r^5(1 - \frac{2m}{r})^2}\right) \right. \\ & \left. + \left(\frac{l^2}{r^2} + hc^2\right) \left(\frac{m(12m^2 + m(-14 + \sqrt{1 - \frac{2m}{r}})r - (5 + \sqrt{1 - \frac{2m}{r}})r^2)}{8r^5(1 - \frac{2m}{r})}\right) \right\} + \mathcal{O}(\Theta^4) \end{aligned} \quad (23)$$

In the commutative limit ($\Theta \rightarrow 0$), the effective potential reduces to the standard Schwarzschild form:

$$V_{\text{eff}}(r, \Theta = 0) = \left(1 - \frac{2m}{r}\right) \left(\frac{l^2}{r^2} + hc^2\right) - \frac{E^2}{c^2}. \quad (24)$$

A. Radial motion of massive particles

Here, we analyze the radial motion of a massive test particle in the NC Schwarzschild spacetime described by Eq. (17). In this context, we set $\dot{\phi} = 0$ and $l = 0$, while assuming $h = 1$ and $c = 1$. Under these conditions, Eq. (22) reduces to:

$$\begin{aligned} \left(\frac{dr}{d\tau}\right)^2 = & E^2 - \left(1 - \frac{2m}{r}\right) - \Theta^2 \left\{ E^2 \left(\frac{m(64m^2 + m(-49 + 13\sqrt{1 - \frac{2m}{r}})r + 2(13 - 3\sqrt{1 - \frac{2m}{r}})r^2)}{16r^5(1 - \frac{2m}{r})^2}\right) \right. \\ & \left. + \left(\frac{m(12m^2 + m(-14 + \sqrt{1 - \frac{2m}{r}})r - (5 + \sqrt{1 - \frac{2m}{r}})r^2)}{8r^5(1 - \frac{2m}{r})}\right) \right\} + \mathcal{O}(\Theta^4). \end{aligned} \quad (25)$$

When $\Theta = 0$, this equation reduces to the classical radial motion equation of a massive particle in Schwarzschild spacetime.

Next, we consider the free-fall motion of a massive particle in the NC Schwarzschild BH geometry. The particle is initially at rest, i.e., $\dot{r} = 0$, at $r = r_0$ when $\tau = 0$. For the proper time in NC spacetime, we set $E = 1$ in Eq. (25) and integrate, yielding:

$$\begin{aligned} \hat{t} = & -\int_{r_0}^r \left(\frac{2m}{r'} - \Theta^2 \left\{ \left(\frac{m(64m^2 + m(-49 + 13\sqrt{1 - \frac{2m}{r'}})r' + 2(13 - 3\sqrt{1 - \frac{2m}{r'}})r'^2)}{16r'^5(1 - \frac{2m}{r'})^2}\right) \right. \right. \\ & \left. \left. + \left(\frac{m(12m^2 + m(-14 + \sqrt{1 - \frac{2m}{r'}})r' - (5 + \sqrt{1 - \frac{2m}{r'}})r'^2)}{8r'^5(1 - \frac{2m}{r'})}\right) \right\} \right)^{-1/2} dr'. \\ = & -\int_{r_0}^r \sqrt{\frac{2m}{r'}} \left(1 - \Theta^2 \frac{r'}{2m} \left\{ \left(\frac{m(64m^2 + m(-49 + 13\sqrt{1 - \frac{2m}{r'}})r' + 2(13 - 3\sqrt{1 - \frac{2m}{r'}})r'^2)}{16r'^5(1 - \frac{2m}{r'})^2}\right) \right. \right. \end{aligned}$$

$$+ \left(\frac{m(12m^2 + m(-14 + \sqrt{1 - \frac{2m}{r'}})r' - (5 + \sqrt{1 - \frac{2m}{r'}})r'^2)}{8r'^5(1 - \frac{2m}{r'})} \right)^{-1/2} dr'. \quad (26)$$

we choose:

$$\epsilon = \Theta^2 \frac{r'}{2m} \left\{ \left(\frac{m(64m^2 + m(-49 + 13\sqrt{1 - \frac{2m}{r'}})r' + 2(13 - 3\sqrt{1 - \frac{2m}{r'}})r'^2)}{16r'^5(1 - \frac{2m}{r'})^2} \right) + \left(\frac{m(12m^2 + m(-14 + \sqrt{1 - \frac{2m}{r'}})r' - (5 + \sqrt{1 - \frac{2m}{r'}})r'^2)}{8r'^5(1 - \frac{2m}{r'})} \right) \right\}, \quad (27)$$

where ϵ is a small parameter, due to the smallness of Θ . Here we can use the first-order approximation of ϵ :

$$(1 - \epsilon)^{-1/2} \approx 1 + \frac{1}{2}\epsilon + \mathcal{O}(\epsilon^2), \quad (28)$$

Using Eq. (28), proper time in equation (26) can be written up to the second order of Θ as

$$\hat{\tau} = - \int_{r_0}^r \left(\sqrt{\frac{r'}{2m}} - \Theta^2 \sqrt{\frac{r'}{2m}} \left\{ \frac{48m^3 - 144m^2r' + 57mr'^2 - 16r'^3 + (4m^2r' - 19mr'^2 + 8r'^3)\sqrt{1 - \frac{2m}{r'}}}{64r'^5(1 - \frac{2m}{r'})^2} \right\} \right) dr'. \quad (29)$$

After integration, the proper time expression up to the second order in Θ is:

$$\begin{aligned} \hat{\tau} = & \frac{2}{3} \left(\sqrt{\frac{r_0^3}{2m}} - \sqrt{\frac{r^3}{2m}} \right) + \Theta^2 \left\{ \sqrt{\frac{r_0}{2m}} \left(\frac{32m^2 + 4m(-52 + \sqrt{1 - \frac{2m}{r_0}})r_0 + 131r_0^2}{128(2m - r_0)r_0^2} \right) \right. \\ & - \sqrt{\frac{r}{2m}} \left(\frac{32m^2 + 4m(-52 + \sqrt{1 - \frac{2m}{r}})r + 131r^2}{128(2m - r)r^2} \right) + \frac{1}{8m} \left(\text{ArcSin} \left(\sqrt{\frac{2m}{r_0}} \right) - \text{ArcSin} \left(\sqrt{\frac{2m}{r}} \right) \right) \\ & \left. + \frac{67}{256m} \left(\text{ArcTanh} \left(\sqrt{\frac{r_0}{2m}} \right) - \text{ArcTanh} \left(\sqrt{\frac{r}{2m}} \right) \right) \right\}. \quad (30) \end{aligned}$$

In the limit $\Theta = 0$, this expression reduced to the commutative case, recovering the classical result.

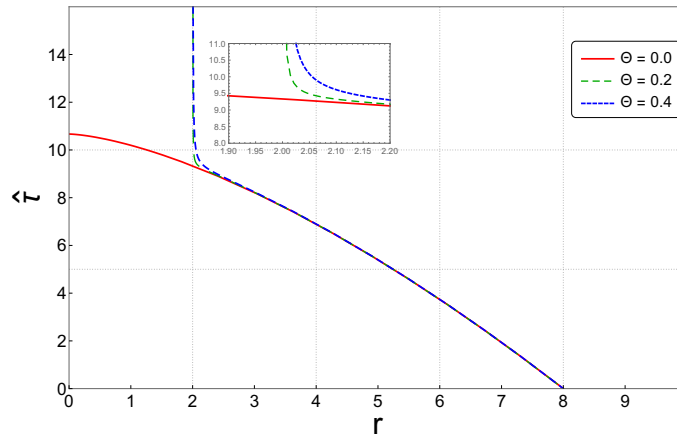


FIG. 1 Proper time evolution for the free fall of a massive particle in the NC Schwarzschild BH as a function of r , with $m = 1$ and the initial position $r_0 = 8$.

Fig. 1 illustrates the variation of proper time $\hat{\tau}$ as a function of r during the free fall of a massive test particle into the NC Schwarzschild BH. The NC parameter Θ significantly influences the proper time near the event horizon,

leading to an increase in its duration. The infinite time is required to reach the NC singularity resulting from non-commutativity effects (see Ref. [54]), and this phenomenon is absent in the commutative case [2].

Similarly to proper time, the coordinate time \hat{t} for the free fall in the NC Schwarzschild BH can be obtained using (20) and (25) together with $E = 1$:

$$\hat{t} = - \int_{r_0}^r (\hat{g}_{tt})^{-1} \left(\frac{2m}{r'} - \Theta^2 \left\{ \left(\frac{m(64m^2 + m(-49 + 13\sqrt{1 - \frac{2m}{r'}})r' + 2(13 - 3\sqrt{1 - \frac{2m}{r'}})r'^2)}{16r'^5(1 - \frac{2m}{r'})^2} \right) + \left(\frac{m(12m^2 + m(-14 + \sqrt{1 - \frac{2m}{r'}})r' - (5 + \sqrt{1 - \frac{2m}{r'}})r'^2)}{8r'^5(1 - \frac{2m}{r'})} \right) \right\}^{-1/2} \right) dr', \quad (31)$$

At leading order in Θ , and integration, the coordinate time is given by:

$$\begin{aligned} \hat{t} = & \frac{2}{3} \left(\sqrt{\frac{r_0^3}{2m}} - \sqrt{\frac{r^3}{2m}} \right) + 4m \left(\sqrt{\frac{r_0}{2m}} - \sqrt{\frac{r}{2m}} \right) - 4m \left(\text{ArcTanh} \left(\sqrt{\frac{r_0}{2m}} \right) - \text{ArcTanh} \left(\sqrt{\frac{r}{2m}} \right) \right) \\ & + \Theta^2 \left\{ \sqrt{\frac{r_0}{2m}} \left(-\frac{25}{16r_0} - \frac{37m}{128(r_0 - 2m)^2} + \frac{15\sqrt{1 - \frac{2m}{r_0}}}{32(r_0 - 2m)^2} - \frac{r_0\sqrt{1 - \frac{2m}{r_0}}}{4(r_0 - 2m)^2} - \frac{61}{512(r_0 - 2m)} \right) \right. \\ & - \sqrt{\frac{r}{2m}} \left(-\frac{25}{16r} - \frac{37m}{128(r - 2m)^2} + \frac{15\sqrt{1 - \frac{2m}{r}}}{32(r - 2m)^2} - \frac{r\sqrt{1 - \frac{2m}{r}}}{4(r - 2m)^2} - \frac{61}{512(r - 2m)} \right) \\ & \left. + \frac{1}{4m} \left(\text{ArcSin} \left(\sqrt{\frac{2m}{r_0}} \right) - \text{ArcSin} \left(\sqrt{\frac{2m}{r}} \right) \right) + \frac{605}{1024m} \left(\text{ArcTanh} \left(\sqrt{\frac{r_0}{2m}} \right) - \text{ArcTanh} \left(\sqrt{\frac{r}{2m}} \right) \right) \right\}. \quad (32) \end{aligned}$$

The commutative expression for the coordinate time is recovered by setting $\Theta = 0$.

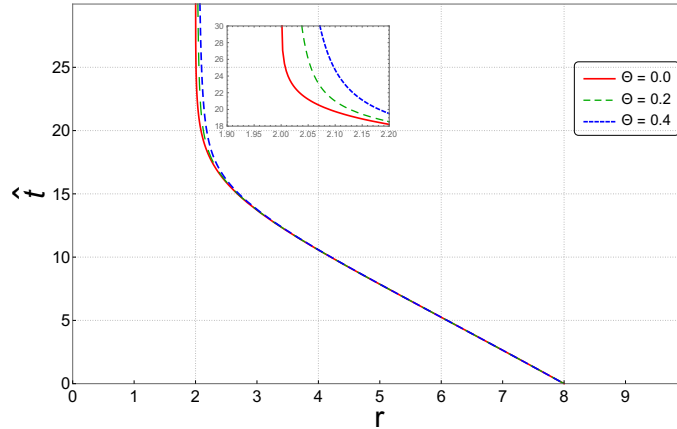


FIG. 2 Coordinate time evolution for the free fall of a massive particle in the NC Schwarzschild BH as a function of r , with $m = 1$ and the initial position $r_0 = 8$.

In Fig. 2, we present the variation of coordinate time \hat{t} during the free fall of a massive test particle in the NC Schwarzschild BH. The effect of non-commutativity becomes significant near the NC event horizon, where it leads to an increase in the coordinate time required for the particle to approach the NC horizon. This qualitative behavior aligns with the commutative case, as discussed in [2], but is further modified due to the presence of non-commutativity.

Fig. 3 depicts the behavior of both proper time and coordinate time for a massive particle falling toward the NC Schwarzschild BH. These results indicate that non-commutativity prevents a massive particle from reaching the NC singularity within a finite time, in contrast to the commutative case [2]. It is noteworthy that in this approach, the commutative case is recovered in the limit $\Theta = 0$, and preserving the expected large-distance commutative behavior

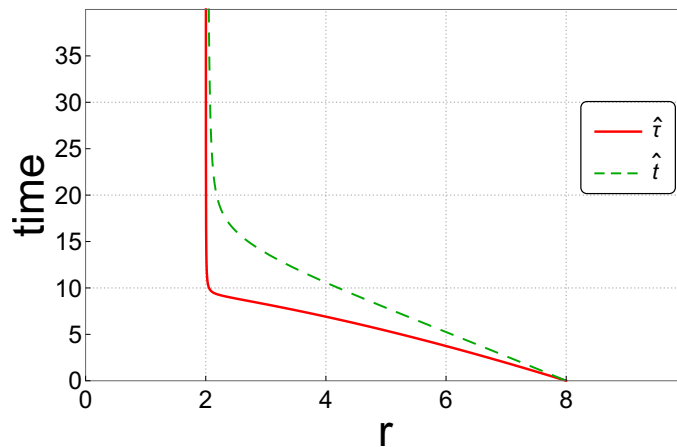


FIG. 3 Comparison of proper and coordinate time for the free fall of a massive particle in the NC Schwarzschild BH as a function of r , with $m = 1$ and the initial position $r_0 = 8$.

while introducing novel effects near the event horizon. This feature is not realized in other approaches [46–48]. Furthermore, the results highlight the impact of utilizing the gauge theory of gravity in NC spacetime to analyze the geodesic motion of test particles.

B. Circular motion of massive particles and Lyapunov exponents

The effective potential governing the dynamics of a massive test particle is given by (23) for $h = 1$, $l \neq 0$, and $c = 1$, and is analyzed in detail in Ref. [54].

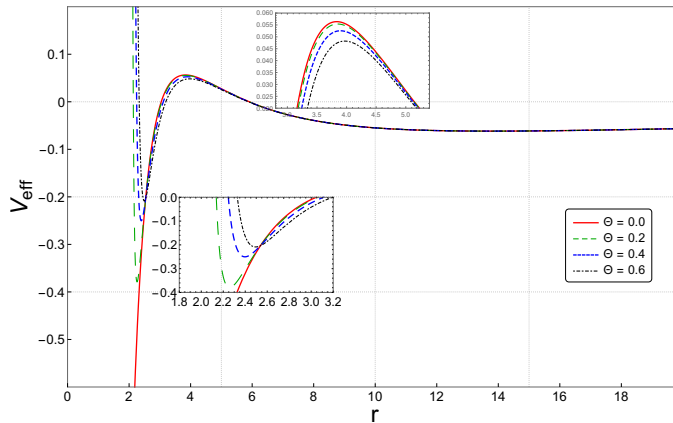


FIG. 4 Effective potential for a massive particle as a function of r , for different values of Θ with fixed parameters: $E = 0.998$, $m = 1$, and $l = 4.2$.

Fig. 4 illustrates the influence of the NC parameter Θ on the effective potential of a massive test particle. Notably, the introduction of non-commutativity generates a new minimum in the effective potential near the event horizon, regardless of the angular momentum values ($l \geq 0$). This new minimum, located outside the event horizon, corresponds to a stable circular orbit [54], leading to the existence of multiple stable circular orbits in NC Schwarzschild geometry. In contrast, prior studies on non-commutativity in geodesic motion—whether based on NC matter distributions [42–48, 50, 51, 72, 73] and on NC gauge theory of gravity via deformed geometry [56, 57] or via deformed mass [58–60] have not predicted these new stable circular orbits near the event horizon.

To assess the stability of these circular orbits, the effective potential must satisfy the following conditions:

$$V_{eff}(r, \Theta) = 0, \quad \frac{dV_{eff}}{dr} = 0. \quad (33)$$

Using these conditions, the leading-order corrections in Θ for the energy E_c^2 and angular momentum L_c^2 of circular orbits are given by:

$$E_c^2 \simeq \frac{(-2m + r_c)^2}{r_c(r_c - 3m)} - \frac{(B(r_c) + F(r_c)\sqrt{1 - \frac{2m}{r_c}})\Theta^2}{32r_c^4(-3m + r_c)^2\sqrt{1 - \frac{2m}{r_c}}} + \mathcal{O}(\Theta^4), \quad (34)$$

$$L_c^2 \simeq \frac{mr_c^2}{r_c - 3m} - \frac{(S(r_c) + Q(r_c)\sqrt{1 - \frac{2m}{r_c}})\Theta^2}{32r_c(-3m + r_c)^2(r_c - 2m)\sqrt{1 - \frac{2m}{r_c}}} + \mathcal{O}(\Theta^4), \quad (35)$$

where the coefficients are defined as:

$$B(r_c) = -120m^4 + 162m^3r_c - 71m^2r_c^2 + 4mr_c^3, \quad F(r_c) = 204m^4 - 174m^3r_c + 41m^2r_c^2 - 4mr_c^3, \quad (36a)$$

$$S(r_c) = -48m^4 + 126m^3r_c - 55m^2r_c^2, \quad Q(r_c) = -120m^4 + 174m^3r_c - 75m^2r_c^2 + 8mr_c^3. \quad (36b)$$

In the limit $\Theta \rightarrow 0$, these expressions reduce to their commutative counterparts for Schwarzschild spacetime.

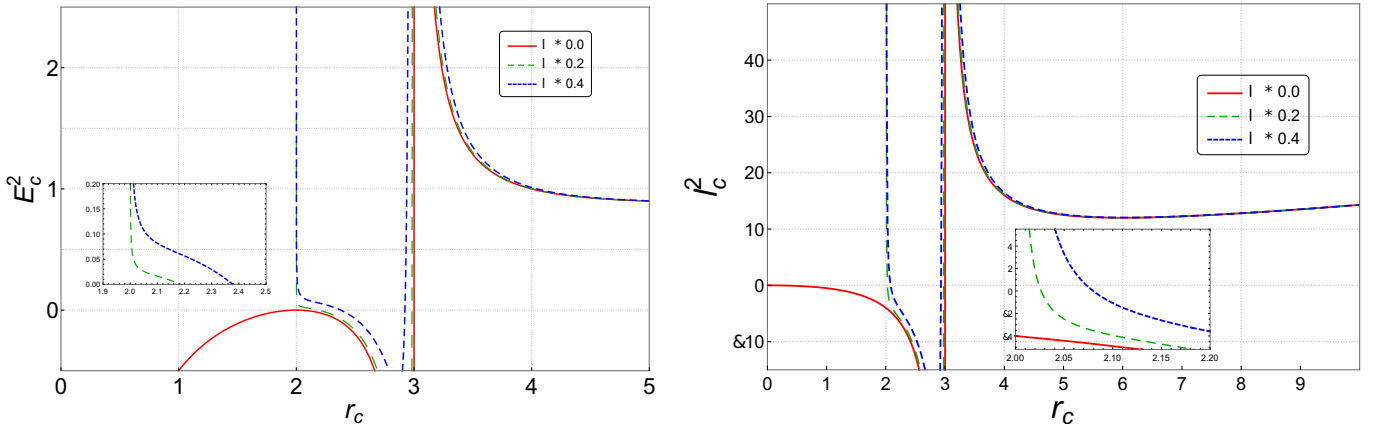


FIG. 5 Energy E_c^2 (left panel) and angular momentum L_c^2 (right panel) for circular orbits of massive particles in NC Schwarzschild spacetime, as functions of r_c .

Fig. 5 presents the behavior of E_c^2 and L_c^2 for circular orbits as functions of r_c , highlighting the impact of the NC parameter Θ . The left panel shows that NC modifications introduce a region near the event horizon where the energy condition becomes unphysical ($E_c^2 < 0$). However, beyond this region, E_c^2 transitions into a physical region ($E_c^2 > 0$), indicating the emergence of a new innermost stable circular orbit (ISCO) in NC geometry [54]. In the right panel, the influence of Θ on angular momentum is evident, with positive values corresponding to the newly formed stable circular orbits near the event horizon. When $\Theta = 0$, these additional features disappear, restoring the classical Schwarzschild behavior.

1. Orbital velocity and time period

The orbital velocity of a massive test particle in the NC Schwarzschild spacetime is defined as [33, 63]:

$$\hat{\Omega}_c = \frac{\dot{\phi}}{\dot{t}}. \quad (37)$$

Utilizing Eqs. (20), (34), and (35), the orbital velocity, accurate to second order in the NC parameter Θ , is given by:

$$\hat{\Omega}_c = \sqrt{\frac{m}{r_c^3} + \frac{X(r_c) + W(r_c)\sqrt{1 - \frac{2m}{r_c}}}{32r_c^6(r_c - 2m)^3}\Theta^2}, \quad (38)$$

where the functions $X(r_c)$ and $W(r_c)$ are defined as:

$$\begin{aligned} X(r_c) &= -1272m^5 + 2304m^4r_c - 1544m^3r_c^2 + 451m^2r_c^3 - 48mr_c^4, \\ W(r_c) &= -192m^4r_c + 298m^3r_c^2 - 137m^2r_c^3 + 24mr_c^4. \end{aligned} \quad (39)$$

In the limit $\Theta = 0$, the commutative Schwarzschild case is recovered [33].

The time period, or orbital times scale of the coordinate time in NC spacetime is given by [33]:

$$\hat{T}_\Omega = \frac{2\pi}{\hat{\Omega}_c}. \quad (40)$$

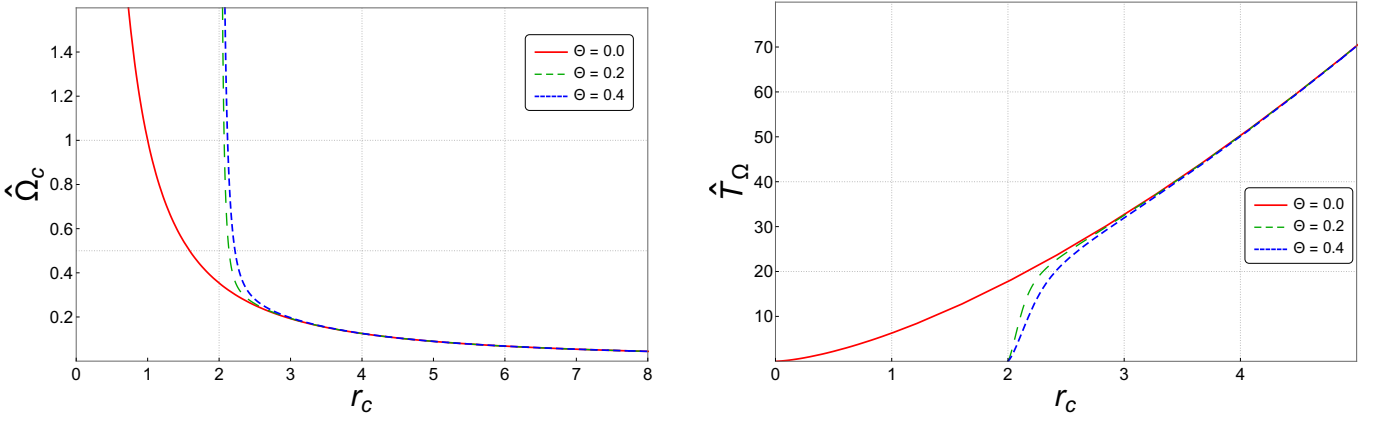


FIG. 6 The behavior of the NC orbital velocity (left panel) and the NC orbital period (right panel) for a massive test particle.

Fig. 6 illustrates the orbital velocity (left panel) and the orbital time scale (right panel) of a massive test particle in NC Schwarzschild spacetime as functions of r_c . The effects of non-commutativity become significant near the NC event horizon r_h^{NC} . Specifically, non-commutativity increases the orbital velocity in the vicinity of r_h^{NC} , while its impact becomes negligible at larger orbital radius. Similarly, the orbital period decreases due to non-commutativity, approaching zero near the NC event horizon. This reduction is most pronounced close to r_h^{NC} and becomes negligible for $r_c \gg 3$, where NC effects vanish.

2. Lyapunov exponents

To analyze the stability and instability of circular geodesics for a massive test particle in the NC Schwarzschild spacetime, we employ the Lyapunov exponents $\hat{\lambda}$. The stability of an orbit is determined by the nature of $\hat{\lambda}$: an imaginary $\hat{\lambda}$ indicates a stable orbit, whereas a real $\hat{\lambda}$ signifies instability [37, 40]. The proper time ($\hat{\lambda}_p$) and coordinate time ($\hat{\lambda}_c$) Lyapunov exponents in NC spacetime are given by [33, 37, 39, 40]:

$$\hat{\lambda}_p = \pm \sqrt{\frac{-V''_{eff}(r, \Theta)}{2}}, \quad \hat{\lambda}_c = \pm \sqrt{\frac{-V''_{eff}(r, \Theta)}{2t^2}}. \quad (41)$$

Using the effective potential (23) along with Eqs. (20), (34), and (35), the Lyapunov exponents are expressed as:

$$\hat{\lambda}_p = \sqrt{-\frac{m(r_c - 6m)}{(r_c - 3m)r_c^3} + \frac{Z(r_c) + P(r_c)\sqrt{1 - \frac{2m}{r_c}}}{32(r_c - 2m)^3r_c^6(r_c - 3m)^2}\Theta^2}, \quad (42)$$

$$\hat{\lambda}_c = \sqrt{-\frac{m(r_c - 6m)}{r_c^4} + \frac{Y(r_c) + N(r_c)\sqrt{1 - \frac{2m}{r_c}}}{32(r_c - 2m)^3 r_c^7} \Theta^2}. \quad (43)$$

The functions $Z(r_c)$, $P(r_c)$, $Y(r_c)$, and $N(r_c)$ are given by:

$$Z(r_c) = 16416m^7 - 38544m^6 r_c + 34992m^5 r_c^2 - 16116m^4 r_c^3 + 4076m^3 r_c^4 - 551m^2 r_c^5 + 32m r_c^6, \quad (44a)$$

$$P(r_c) = 3564m^6 r_c - 8058m^5 r_c^2 + 7070m^4 r_c^3 - 2910m^3 r_c^4 + 517m^2 r_c^5 - 24m r_c^6, \quad (44b)$$

$$Y(r_c) = 8880m^6 - 16568m^5 r_c + 11200m^4 r_c^2 - 3470m^3 r_c^3 + 515m^2 r_c^4 - 32m r_c^5, \quad (44c)$$

$$N(r_c) = 1668m^5 r_c - 2870m^4 r_c^2 + 1808m^3 r_c^3 - 473m^2 r_c^4 + 24m r_c^5. \quad (44d)$$

In the limit $\Theta = 0$, the commutative Schwarzschild case is recovered [37, 39].

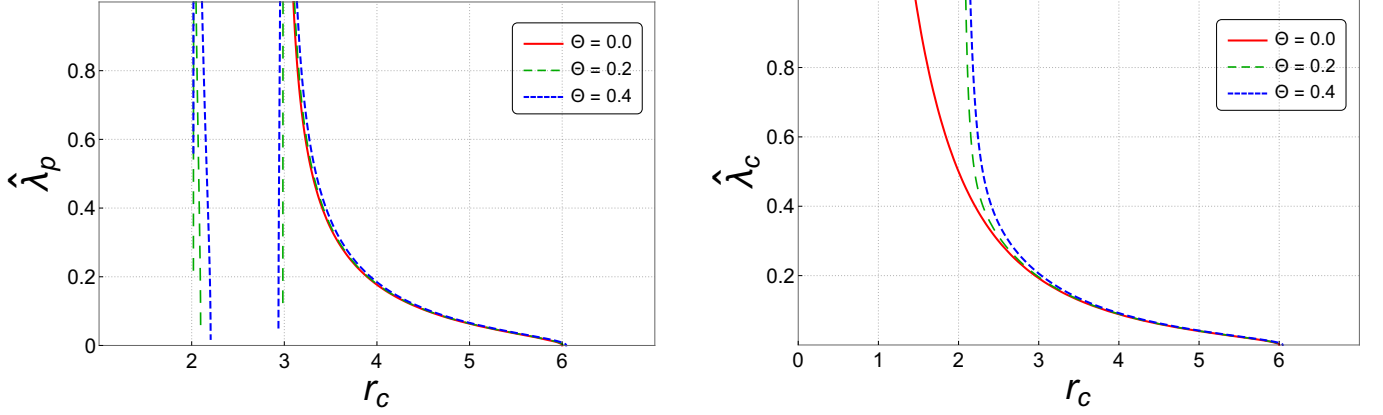


FIG. 7 Proper time (left panel) and coordinate time (right panel) Lyapunov exponents for a massive particle as functions of the circular orbit radius r_c .

Fig. 7 illustrates the proper time (left panel) and coordinate time (right panel) Lyapunov exponents for a massive test particle in NC spacetime. The coordinate time Lyapunov exponent $\hat{\lambda}_c$ is real in the region $r_h^{NC} < r_c \leq r_{outer}^{ISCO}$, indicating unstable orbits near the event horizon. As the orbit radius r_c increases, the instability decreases, and reaching zero at the outer ISCO, r_{outer}^{ISCO} . The proper time Lyapunov exponent $\hat{\lambda}_p$ exhibits a distinct behavior: instability (real values) is observed in two regions, $r_h^{NC} < r_c \leq r_{inner}^{ISCO}$ and $r_c^{uns} < r_c \leq r_{outer}^{ISCO}$. Between these intervals, in the range $r_{inner}^{ISCO} \leq r_c \leq r_c^{uns}$, $\hat{\lambda}_p$ becomes imaginary, indicating stability of the circular orbit. These results confirm the existence of new stable circular orbits near the event horizon, consistent with previous findings [54].

The ratio of the proper time to coordinate time Lyapunov exponents is given by:

$$\frac{\hat{\lambda}_p}{\hat{\lambda}_c} = \sqrt{\frac{r_c}{r_c - 3m} + \frac{Y(r_c)(3m - r_c) - Z(r_c) + (N(r_c)(3m - r_c) - P(r_c))\sqrt{1 - \frac{2m}{r_c}}}{32m(r_c - 2m)^3 (r_c - 3m)^2 (r_c - 6m)r_c^2} \Theta^2}. \quad (45)$$

In the limit $\Theta = 0$, the commutative case is recovered [37, 39].

Fig. 8 illustrates the ratio $\hat{\lambda}_p/\hat{\lambda}_c$ as a function of r_c in NC spacetime. The ratio remains real in two distinct regions, separated by an interval where it becomes imaginary, reflecting the behavior observed in the proper time Lyapunov exponent. The analysis of proper time and coordinate time Lyapunov exponents, along with their ratio, reveals a novel feature in the dynamics of circular motion around an NC Schwarzschild BH. Specifically, it predicted a new range of stable circular orbits located between unstable ones.

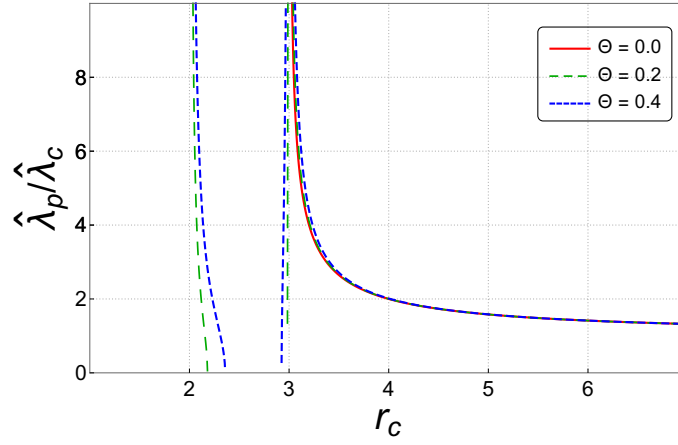


FIG. 8 The ratio of proper time to coordinate time Lyapunov exponents for a massive test particle in NC Schwarzschild spacetime as a function of r_c .

C. Radial motion of massless particles

The radial motion of massless particles in the NC Schwarzschild spacetime can be derived using the effective potential (23) by setting $h = 0$, $c = 0$, and $l = 0$. This leads to the equation governing radial motion:

$$\left(\frac{dr}{d\tau}\right)^2 = E^2 - \Theta^2 \left\{ E^2 \frac{m(64m^2 + m(-49 + 13\sqrt{1 - \frac{2m}{r}})r + 2(13 - 3\sqrt{1 - \frac{2m}{r}})r^2)}{16r^5 (1 - \frac{2m}{r})^2} \right\} + \mathcal{O}(\Theta^4), \quad (46)$$

where the commutative case is recovered when $\Theta = 0$.

For a photon freely falling toward the NC Schwarzschild BH and emitted from a radial position $r = r_0$ with energy $E = 1$, the affine parameter τ and coordinate time \hat{t} are given by:

$$\hat{\tau} = - \int_{r_0}^r \left[1 - \Theta^2 \frac{m(64m^2 + m(-49 + 13\sqrt{1 - \frac{2m}{r}})r + 2(13 - 3\sqrt{1 - \frac{2m}{r}})r^2)}{16r^5 (1 - \frac{2m}{r})^2} \right]^{-\frac{1}{2}} dr, \quad (47)$$

$$\hat{t} = - \int_{r_0}^r (\hat{g}_{00})^{-1} \left[1 - \Theta^2 \frac{m(64m^2 + m(-49 + 13\sqrt{1 - \frac{2m}{r}})r + 2(13 - 3\sqrt{1 - \frac{2m}{r}})r^2)}{16r^5 (1 - \frac{2m}{r})^2} \right]^{-\frac{1}{2}} dr. \quad (48)$$

By evaluating these integrals to leading order in Θ , the results are:

$$\begin{aligned} \hat{\tau} = r_0 - r + \Theta^2 \left\{ 25 \ln \left(\frac{r_0(r-2m)}{r(r_0-2m)} \right) - \frac{1}{128m} \left[\frac{32m^2 + 15mr_0 + 8r_0^2}{r_0^2} - \frac{32m^2 + 15mr + 8r^2}{r^2} \right] \right. \\ \left. + \frac{1}{128m} \left[\left(1 - \frac{2m}{r}\right)^{-\frac{1}{2}} - \left(1 - \frac{2m}{r_0}\right)^{-\frac{1}{2}} - 14 \left(\sqrt{1 - \frac{2m}{r}} - \sqrt{1 - \frac{2m}{r_0}} \right) \right. \right. \\ \left. \left. - \frac{13}{3} \left(\left(1 - \frac{2m}{r}\right)^{\frac{3}{2}} - \left(1 - \frac{2m}{r_0}\right)^{\frac{3}{2}} \right) - \frac{35}{2} \frac{r_0(r-2m) - r(r_0-2m)}{(r_0-2m)(r-2m)} \right] \right\}, \quad (49) \end{aligned}$$

$$\begin{aligned} \hat{t} = r_0 - r + 2m \ln \left(\frac{r_0 - 2m}{r - 2m} \right) + \Theta^2 \left\{ - \frac{224m^2 - 201mr_0 + 63r_0^2}{128r_0(r_0 - 2m)^2} + \frac{224m^2 - 201mr + 63r^2}{128r(r - 2m)^2} \right. \\ \left. - \frac{(17m^2 - 24mr_0 + 8r_0^2)\sqrt{1 - \frac{2m}{r_0}}}{m(r_0 - 2m)^2} + \frac{(17m^2 - 24mr + 8r^2)\sqrt{1 - \frac{2m}{r}}}{m(r - 2m)^2} - \frac{63}{m} \ln \left(\frac{r_0(r - 2m)}{r(r_0 - 2m)} \right) \right\}. \quad (50) \end{aligned}$$

The commutative limits of the affine parameter and coordinate time are recovered by setting $\Theta = 0$ [2].

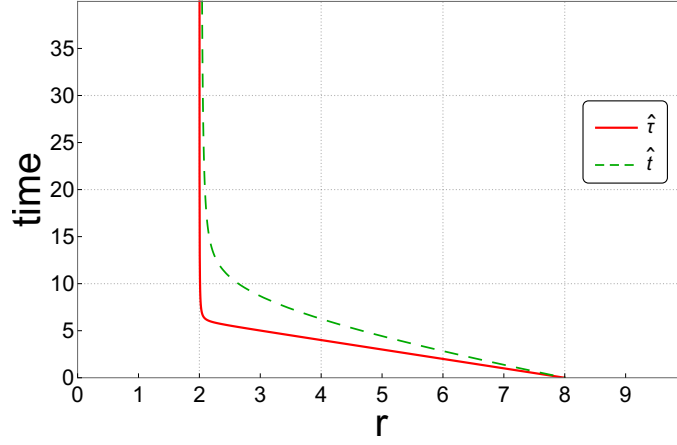


FIG. 9 Variation of the affine parameter \hat{t} and coordinate time \hat{t} along a radial null geodesic of a photon in NC Schwarzschild spacetime as a function of r .

Fig. 9 illustrates the behavior of \hat{t} and \hat{t} for a photon initially at $r = r_0$ falling toward the NC Schwarzschild BH. Notably, in the affine parameter framework of NC spacetime, photons require an infinite affine parameter to reach the NC singularity, in contrast to the commutative case [2, 74]. The same observation applies to coordinate time, where the photon cannot reach the singularity within a finite time. This behavior is consistent with the motion of massive particles and highlights the role of non-commutativity in preventing singularity encounters within a finite temporal or affine framework. Additionally, for massless particles, our analysis predicts a novel behavior in free-fall motion within NC spacetime using the NC gauge theory of gravity. This differs from the approach in Refs. [47, 48], which alters the commutative behavior and modifies the underlying physics of the spacetime geometry. In contrast, non-commutativity should act as a quantum correction to the metric, reducing to the commutative case when this correction vanishes. While using an NC matter distribution can recover the commutative free-fall motion, as demonstrated in Ref. [44], it does not introduce any new predictions for free-fall dynamics. However, our approach based on the NC gauge theory of gravity preserves the commutative solution while predicting new macroscopic effects of non-commutativity.

D. Circular motion of massless particles and Lyapunov exponents

This section examines the null geodesic motion of photons around an NC Schwarzschild black hole (BH). The effective potential for a photon in this spacetime is obtained from (23) by setting $h = 0$, $c = 1$ and $l \neq 0$.

Fig. 10 illustrates the influence of the NC parameter Θ (left panel) and the angular momentum l (right panel) on the effective potential of a massless test particle (photon). As shown in the left panel, introducing non-commutativity leads to the emergence of a new minimum in the effective potential close to the event horizon. This phenomenon is analogous to what is observed for massive test particles (see SubSec. III B). However, for massless particles, only two extrema of the effective potential exist outside the event horizon, allowing the interpretation of the new minimum as a stable circular orbit. This results in the formation of a stable photon sphere in this spacetime. Additionally, the position of this new minimum shifts farther from the event horizon as Θ increases. Moreover, the influence of non-commutativity becomes negligible in regions significantly distant from the event horizon ($r \gg r_h^{NC}$). The right panel of Fig. 10 reveals that in NC spacetime, the effective potential exhibits extremal points only for angular momentum values that satisfy a specific condition. This contrasts with the commutative case, where the effective potential always possesses a maximum, irrespective of the angular momentum. For $\Theta = 0.2$, the effective potential exhibits two extrema when the angular momentum exceeds a critical value, $l^{\text{crit}} \geq 2.55$. These critical values depend on the NC parameter Θ . In conclusion, NC spacetime consistently supports the existence of two photon spheres: an inner stable photon sphere and an outer unstable photon sphere. This behavior differs significantly from the commutative case and highlights the unique role of NC geometry in modifying the geodesic structure of spacetime. Furthermore, these results are novel and distinct from previous works [44, 47, 48, 50, 56–60], which could not predict the existence of a new stable photon sphere near the event horizon.

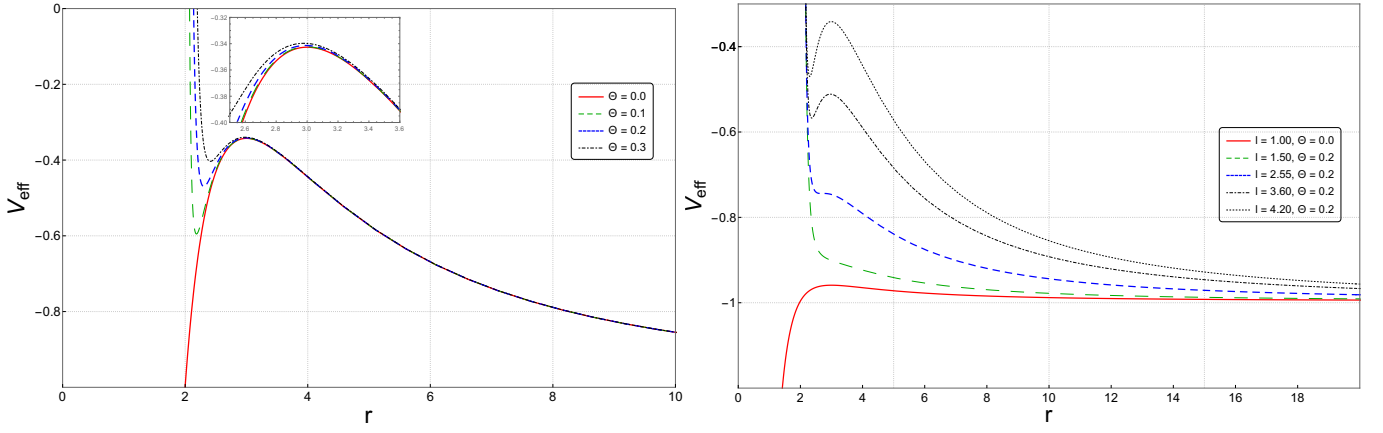


FIG. 10 Behavior of the effective potential for a massless particle with varying non-commutative parameter Θ and fixed values of $E = 0.998$, $m = 1$, $l = 4.2$ (left panel), and with varying angular momentum l and fixed $E = 0.998$, $m = 1$, $\Theta = 0.2$ (right panel).

1. Null circular orbit and photon sphere

The conditions for the circular motion of photons in NC Schwarzschild spacetime are analogous to those for massive particles, as given in (33). By utilizing the effective potential (23) with $h = 0$, the relationship between the photon's energy E_c and angular momentum L_c can be expressed as:

$$\frac{1}{D_c} = \frac{E_c}{L_c} = \sqrt{\frac{r_c - 2m}{r_c^3} + \left(\frac{J(r_c) + G(r_c)\sqrt{1 - \frac{2m}{r_c}}}{16r_c^6(r_c - 2m)} \right) \Theta^2}, \quad (51)$$

where D_c is the impact parameter, and the functions $J(r_c)$ and $G(r_c)$ are defined as:

$$J(r_c) = 156m^3 - 185m^2r_c + 73mr_c^2 - 10r_c^3, \quad G(r_c) = 33m^2r_c - 37mr_c^2 + 6r_c^3. \quad (52)$$

TABLE I Numerical values for the unstable r_{uns} and the new stable circular orbit r_{sta} of the photon sphere in NC spacetime for different Θ values, with $E = 0.998$, $l = 4.2$, and $m = 1$.

Θ	0	0.10	0.15	0.20	0.25	0.30
r_{sta} (new)	2.18400	2.24624	2.30383	2.35865	2.41183	
r_{uns}	3.00000	2.99782	2.99504	2.99101	2.98559	2.97855

Table I presents numerical solutions of (33), illustrating the dependence of the stable and unstable photon sphere radii on Θ . For $3.29 \leq l \leq 4.48$ (where this condition depends on $0 \leq \Theta \leq 0.3$), the stable circular orbit radius increases with Θ , while the unstable orbit radius decreases. However, for $l > 4.48$, both orbit radii increase as Θ grows.

The left panels of Fig. 11 demonstrate that as Θ increases, the radius of the stable circular orbit grows, while the radius of the unstable orbit decreases. In the NC framework, the unstable photon orbit has a smaller radius than in the commutative case for $l < 4.48$, whereas for $l \geq 4.48$, the unstable orbit radius exceeds the commutative value. This divergence arises from modifications to the gravitational field induced by non-commutativity. The right panels of Fig. 11 illustrate the dependence of circular orbit radii on angular momentum l . For a fixed $\Theta = 0.3$, the stable circular orbit radius decreases as l increases, while the unstable orbit radius grows. This behavior reflects the distinctive interplay between angular momentum and the NC parameter in shaping the geodesic structure of spacetime.

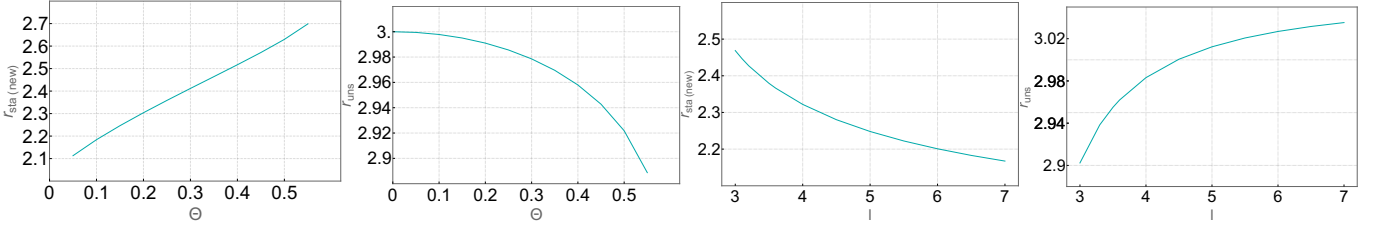


FIG. 11 Behavior of the photon sphere radius in NC spacetime. Stable and unstable circular orbits are shown as functions of Θ for fixed $l = 4.2$, $E = 1$, $m = 1$ (two left panels), and as functions of l for fixed $\Theta = 0.3$, $E = 1$, $m = 1$ (two right panels).

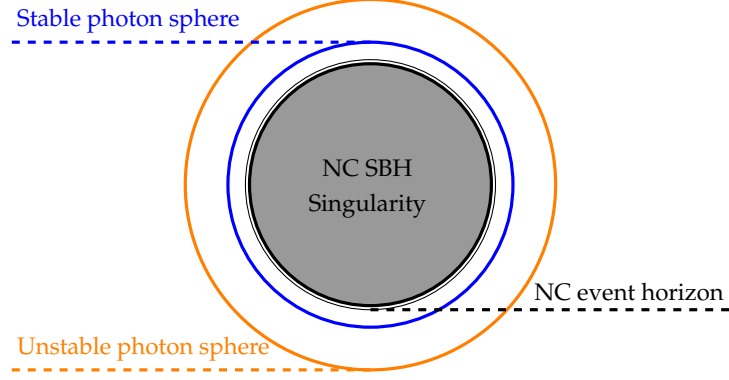


FIG. 12 The schematic picture of the stable/unstable photon sphere around the NC SBH.

2. Lyapunov exponents

In the following, we analyze the stability and instability of the two photon spheres in NC spacetime using the Lyapunov exponent. As is well known, for null circular orbits of photons, proper time does not exist, leaving only the coordinate time Lyapunov exponent for analysis.

We begin by calculating the angular frequency and the period in coordinate time, as given by equations (37) and (40), respectively:

$$\hat{\Omega}_c^{\text{Null}} = \frac{1}{D_c}, \quad \hat{T}_{\hat{\Omega}}^{\text{Null}} = 2\pi D_c. \quad (53)$$

Next, the coordinate time Lyapunov exponent for photon orbits around the NC Schwarzschild BH is derived as:

$$\hat{\lambda}_c^{\text{Null}} = \sqrt{-\frac{3((-4m+r_c)(-2m+r_c))}{r_c^4} + \left(\frac{O(r_c) + I(r_c)\sqrt{1-\frac{2m}{r_c}}}{32(r_c-2m)^2 r_c^7}\right)^2} \Theta^2, \quad (54)$$

where

$$O(r_c) = -19488m^5 + 39000m^4 r_c - 29076m^3 r_c^2 + 9958m^2 r_c^3 - 1716m r_c^4 + 140r_c^5, \quad (55a)$$

$$I(r_c) = -3171m^4 r_c + 5773m^3 r_c^2 - 3908m^2 r_c^3 + 1080m r_c^4 - 84r_c^5. \quad (55b)$$

Fig. 13 illustrates the behavior of the coordinate time Lyapunov exponent for photons as a function of r_c (left panel) and Θ (right panel). The left panel shows that instability initially increases to a peak (decreasing with higher Θ), then decreases as r_c increases, eventually vanishing for $r_c \geq 4$. In NC spacetime, orbits near the event horizon exhibit reduced instability compared to the commutative case, whereas at larger distances from the event horizon, this trend reverses. Moreover, while instability begins at the event horizon in commutative spacetime, NC geometry shifts it outward, allowing for the presence of stable orbits near the event horizon. This observation is consistent with the effective potential analysis for massless test particles, confirming the existence of a stable photon sphere around the NC Schwarzschild BH. Similar behavior has been reported in other NC geometries, as discussed in Ref. [63],

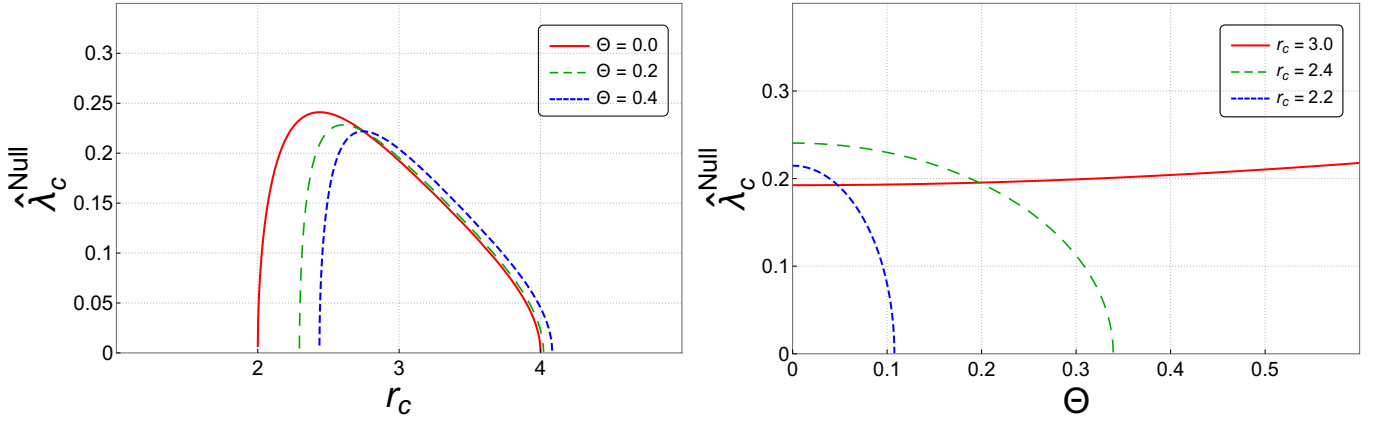


FIG. 13 Coordinate time Lyapunov exponent for massless particles as a function of r_c (left panel) and the NC parameter Θ (right panel).

where orbits within the event horizon cannot form a stable photon sphere. Examining the dependence of circular orbit radii r_c on Θ (right panel) reveals that the orbit at $r_c = 3$ remains unstable in NC spacetime, with increasing Θ amplifying this instability. In contrast, the new circular orbits emerging near the event horizon in NC spacetime exhibit reduced instability, which decreases as Θ increases and eventually stabilizes. This suggests the existence of stable circular orbits near the event horizon in NC spacetime.

The ratio of the Lyapunov exponent to the angular frequency in coordinate time ($\frac{\hat{\lambda}_c^{\text{Null}}}{\hat{\Omega}_c^{\text{Null}}}$) defines the instability exponent of null circular orbits in NC spacetime:

$$\frac{\hat{\lambda}_c^{\text{Null}}}{\hat{\Omega}_c^{\text{Null}}} = \sqrt{\frac{3(4m - r_c)}{r_c} + \left(\frac{O(r_c) + 6J(r_c)(8m^2 - 6mr_c + r_c^2) + (I(r_c) + 6G(r_c)(8m^2 - 6mr_c + r_c^2))\sqrt{1 - \frac{2m}{r_c}}}{32(r_c - 2m)^3 r_c^4} \right) \Theta^2}. \quad (56)$$

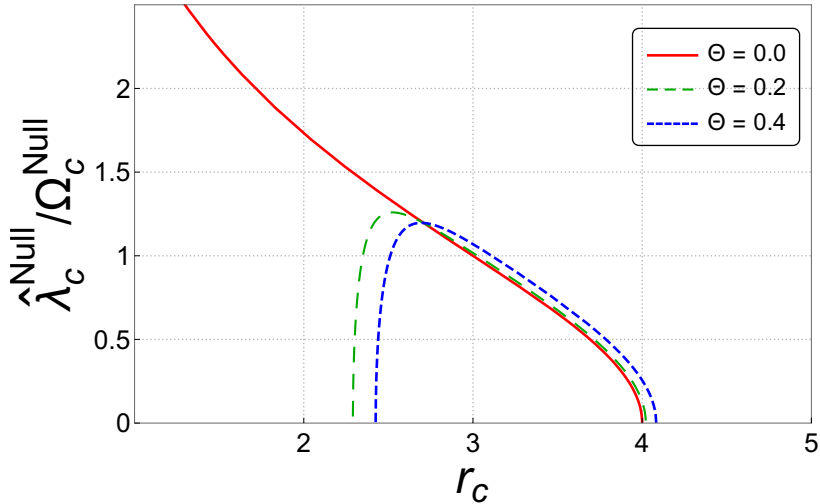


FIG. 14 Ratio of the Lyapunov exponent to the angular frequency in coordinate time as a function of r_c .

Fig. 14 illustrates the variation of $\hat{\lambda}_c^{\text{Null}}/\hat{\Omega}_c^{\text{Null}}$ with r_c , showing behavior similar to that in Fig. 13. Unlike the commutative case, NC spacetime allows for stable orbits near the event horizon, in contrast to the results in Ref. [63], which confirm the stability of the new photon sphere.

Finally, the critical exponent $\hat{\gamma}$ for null circular orbits is defined as the ratio of the Lyapunov timescale $\hat{T}_\lambda = \frac{2\pi}{\hat{\lambda}}$ to

the orbital timescale $\hat{T}_{\hat{\Omega}} = \frac{2\pi}{\hat{\Omega}}$ [31–33]:

$$\hat{\gamma}^{\text{Null}} = \frac{\hat{T}_{\hat{\lambda}}^{\text{Null}}}{\hat{T}_{\hat{\Omega}}^{\text{Null}}} = \frac{1}{2\pi \sqrt{\frac{3(4m-r_c)}{r_c} + \left(\frac{O(r_c)+6J(r_c)(8m^2-6mr_c+r_c^2)+(I(r_c)+6G(r_c)(8m^2-6mr_c+r_c^2))\sqrt{1-\frac{2m}{r_c}}}{32(r_c-2m)^3r_c^4} \right) \Theta^2}}. \quad (57)$$

In the limit $\Theta = 0$, we recover the commutative case.

TABLE II Critical exponent $\hat{\gamma}^{\text{Null}}$ for unstable orbits r_{uns} and stable orbits r_{sta} of the photon sphere in NC spacetime for different values of Θ , with $m = 1$.

Θ	$r_c = 3$	$r_c = 2.4$	$r_c = 2.3$	$r_c = 2.2$
$\hat{\gamma}^{\text{Null}}$ 0.0	0.159155	–	–	–
0.1	0.158439	0.117291	0.121293	0.251639
0.2	0.156349	0.136225	0.328429	0 – 0.0662942i
0.3	0.153042	0.210585	0 – 0.10626i	0 – 0.0397438i
0.4	0.148746	0 – 0.216564i	0 – 0.0665877i	0 – 0.0288573i

The numerical values of the critical exponent $\hat{\gamma}^{\text{Null}}$ for photons in various circular orbits r_c and different values of the non-commutative (NC) parameter Θ are summarized in Table II. This table highlights the presence of both real and imaginary values of $\hat{\gamma}^{\text{Null}}$. Real positive values indicate unstable circular orbits [32], whereas imaginary values correspond to stable circular orbits. For the photon sphere orbit in the Schwarzschild BH spacetime at $r_c = 3$, instability persists even in the NC framework. According to the definition in Eq. (57), this implies that the Lyapunov timescale $\hat{T}_{\hat{\lambda}}$ is shorter than the orbital timescale $\hat{T}_{\hat{\Omega}}$, i.e., $\hat{T}_{\hat{\lambda}} < \hat{T}_{\hat{\Omega}}$ [31]. A similar behavior is observed for other values of r_c in Table II, where real values of $\hat{\gamma}^{\text{Null}}$ consistently signify instability. Furthermore, the impact of the NC parameter Θ on $\hat{\gamma}^{\text{Null}}$ is evident. As Θ increases, the values of $\hat{\gamma}^{\text{Null}}$ decrease for $r_c = 3$, indicating increasing instability. The smallest values of $\hat{\gamma}^{\text{Null}}$ correspond to stronger Lyapunov instability [33] (see the right panel of Fig. 13). On the other hand, the imaginary values of $\hat{\gamma}^{\text{Null}}$, which denote stable circular orbits, align with the new minima in the effective potential observed for $l = 5.2$ (values comparable to those in Table I). This demonstrates the emergence of a new stable photon sphere in NC spacetime, contrasting with the instability of the external photon sphere in both commutative and NC scenarios.

3. Black hole shadow

In the equatorial plane ($\theta = \pi/2$), the radius of the BH shadow, \hat{R}_{shadow} , is directly related to the impact parameter D_c by the relation $\hat{R}_{\text{shadow}} = D_c|_{r=r_{\text{ps}}}$, where $r_{\text{ps}}^{\text{uns}}$ represents the radius of the unstable photon sphere. This radius can be determined by solving the equation $\frac{dV_{\text{eff}}}{dr} = 0$. To leading order in the NC parameter Θ and the BH mass m , the solution is given by:

$$r_{\text{ps}}^{\text{uns}} = 3m - \left(\frac{-38 + 540D_c^2m^2}{288m} \right) \Theta^2. \quad (58)$$

It is important to note that the radius of the stable photon sphere in NC spacetime can only be obtained numerically (see Table II). Using the above expression, the shadow radius of the NC Schwarzschild BH can be expressed as:

$$\hat{R}_{\text{shadow}} = 3\sqrt{3}m \left(1 + \frac{(1 + 2\sqrt{3})}{72m^2} \Theta^2 \right), \quad (59)$$

where the corresponding commutative case is recovered by setting $\Theta = 0$.

Fig. 15 illustrates the shadow of the NC Schwarzschild BH for different values of the NC parameter Θ (left panel) and the BH mass m (right panel). As seen in the left panel, the shadow radius increases with increasing Θ . Similarly, the right panel shows that for a fixed NC parameter, the shadow radius grows as the BH mass m increases. This behavior suggests that the effects of non-commutativity and BH mass on the shadow radius are analogous. The NC

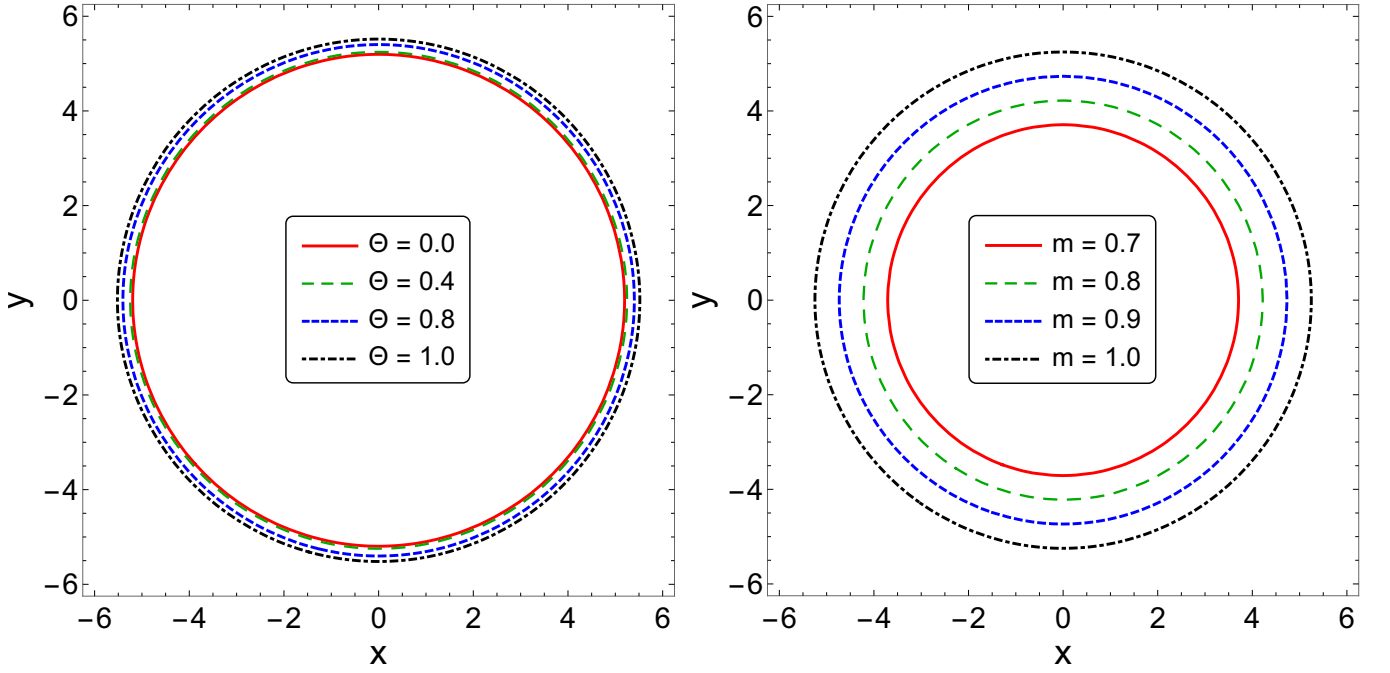


FIG. 15 The shadow of the Schwarzschild BH in NC spacetime for different values of the NC parameter Θ (left panel) with $m = 1$, and for varying BH mass m (right panel) with $\Theta = 0.4$.

parameter influences the spacetime geometry in a way that mimics an increase in mass, effectively strengthening the gravitational field. This conclusion is consistent with our earlier results [54]. Furthermore, we observe that the shadow radius of the NC Schwarzschild BH is larger and exhibits a slight increase with increasing Θ , in contrast to the findings in [75], where it was reported to increase significantly with increasing Θ .

Armed with the above result and considering the constraint on the NC parameter—namely, that the NC correction must be smaller than the precision of the experimental measurement we choose as an implementation of the NC shadow radius of the Schwarzschild BH. Specifically, we consider a typical primordial BH at the final stage of inflation with a mass of $GM \sim 5 \times 10^{-5}m$ [76] and a volume of $r \sim 1.5 \times 10^{-4}m$. Moreover, the precision of the experimental measurement, according to [77], is approximately ~ 0.1 . Consequently, the upper limit of the NC parameter can be determined as:

$$\left| \frac{R_{\text{shadow}} - \hat{R}_{\text{shadow}}}{R_{\text{shadow}}} \right| = \sqrt{3} \frac{(1 + 2\sqrt{3})}{24m} \Theta^2 \leq 0.1. \quad (60)$$

According to Ref. [78], the physical distance measured at any time after inflation can be obtained by multiplying our results by the square of the cosmological scale factor, $a = 10^{-29}$. This is due to our choice of the space-space NC matrix. By applying the above constraint to our system, we find that the NC parameter satisfies:

$$\Theta^{\text{Phys}} = \sqrt{a^2 \Theta^2} \leq 3.94 \times 10^{-32} \text{ m}. \quad (61)$$

It is evident that the obtained result is close to the Planck scale and is consistent with the bounds derived in our previous works, where similar constraints were obtained through experimental tests of gravity in the context of the NC gauge theory of gravity [54, 55] or by employing the Bopp's shift transformation [53, 79, 80]. These studies suggest a bound in the range of $(10^{-34} - 10^{-31})$ m. Remarkably, in this work, the estimation of the NC parameter is directly related to the accuracy of the experimental measurement of the BH shadow radius. This implies that as the precision of the measurement improves, the estimation of the NC parameter can become more refined. A similar observation was made in Ref. [55], where variations in experimental accuracy led to different values of the NC parameter.

IV. CONCLUSIONS

In this study, we examined the geodesic motion of both massive and massless test particles in the NC Schwarzschild spacetime. Our approach was based on modifying the Schwarzschild BH metric using the NC gauge theory of gravity [54]. We computed corrections to the effective potential up to second order in Θ and obtained modifications to both the affine parameter and the coordinate time in the NC Schwarzschild BH. Our results indicate that due to the influence of non-commutativity, both massive and massless particles require an infinite amount of time to reach either the NC singularity or the NC event horizon.

Furthermore, we analyzed the stability of geodesic motion by utilizing the Lyapunov exponent to assess the stability of circular orbits for both massive and massless particles. For massive particles, we determined the angular frequency $\hat{\Omega}_c$, the time period \hat{T}_c , and both the proper-time and coordinate-time Lyapunov exponents, $\hat{\lambda}_p$ and $\hat{\lambda}_c$, respectively. Notably, the proper-time Lyapunov exponent revealed the presence of a stable orbital region between two unstable regions near the event horizon, which aligns with previous findings [54]. For massless particles, our analysis of the effective potential uncovered a novel type of motion near the event horizon, indicating the presence of a stable circular orbit. As a result, a second photon sphere emerges in NC spacetime. Consequently, the NC Schwarzschild BH features two distinct photon spheres: a stable inner photon sphere and an unstable outer photon sphere. By employing the coordinate-time Lyapunov exponent $\hat{\lambda}_c^{\text{Null}}$, we confirmed the instability of the outer photon sphere, while the inner photon sphere remains stable—a feature unique to NC spacetime. Additionally, we computed the critical exponent $\hat{\gamma}^{\text{Null}}$ to further evaluate the instability of null circular orbits in the NC Schwarzschild BH.

Lastly, we explored the impact of non-commutativity on the BH shadow. Our results suggest a resemblance between the effects of mass and non-commutativity, implying that non-commutativity strengthens the gravitational field of the BH. Key insights from our analysis include the connection between newly identified stable circular orbits near the event horizon and non-commutative effects, as well as an estimated upper bound on the NC parameter, which is approximately $\Theta^{\text{Phy}} \sim 10^{-32}$ m.

Acknowledgments

This work is supported by project B00L02UN050120230003, Univ. Batna 1, Algeria.

-
- [1] Aleksandr Mikhailovich Lyapunov. The general problem of the stability of motion. *International Journal of Control*, 55(3):531–534, 1992.
 - [2] Subrahmanyan Chandrasekhar. *The Mathematical Theory of Black Holes*. Oxford University Press, 1999.
 - [3] G. W. Gibbons, C. M. Warnick, and M. C. Werner. Light bending in schwarzschild–de sitter: Projective geometry of the optical metric. *Classical and Quantum Gravity*, 25(24):245009, 2008.
 - [4] J. N. Islam. The cosmological constant and classical tests of general relativity. *Physics Letters A*, 97(6):239–241, 1983.
 - [5] M. J. Jaklitsch, Charles Hellaby, and D. R. Matravers. Particle motion in the spherically symmetric vacuum solution with positive cosmological constant. *General Relativity and Gravitation*, 21(9):941–951, 1989.
 - [6] Zdeněk Stuchlík and Massimo Calvani. Null geodesics in black hole metrics with non-zero cosmological constant. *General Relativity and Gravitation*, 23(5):507–519, 1991.
 - [7] G. V. Kraniotis and S. B. Whitehouse. Compact calculation of the perihelion precession of mercury in general relativity, the cosmological constant and jacobi’s inversion problem. *Classical and Quantum Gravity*, 20(22):4817, 2003.
 - [8] G. V. Kraniotis. Precise relativistic orbits in kerr and kerr–(anti) de sitter spacetimes. *Classical and Quantum Gravity*, 21(19):4743, 2004.
 - [9] Norman Cruz, Marco Olivares, and José R. Villanueva. The geodesic structure of the schwarzschild anti-de sitter black hole. *Classical and Quantum Gravity*, 22(6):1167, 2005.
 - [10] Eva Hackmann, Valeria Kagramanova, Jutta Kunz, and Claus Lämmerzahl. Analytic solutions of the geodesic equation in higher dimensional static spherically symmetric spacetimes. *Physical Review D*, 78(12):124018, 2008.
 - [11] Valeria Kagramanova, Jutta Kunz, Eva Hackmann, and Claus Lämmerzahl. Analytic treatment of complete and incomplete geodesics in taub-nut space-times. *Physical Review D*, 81(12):124044, 2010.
 - [12] Eva Hackmann, Claus Lämmerzahl, Valeria Kagramanova, and Jutta Kunz. Analytical solution of the geodesic equation in kerr–(anti-) de sitter space-times. *Physical Review D*, 81(4):044020, 2010.
 - [13] Eva Hackmann, V. Kagramanova, J. Kunz, and C. Lämmerzahl. Analytic solutions of the geodesic equation in axially symmetric space-times. *EPL (Europhysics Letters)*, 88(3):30008, 2009.
 - [14] Janna Levin and Gabe Perez-Giz. A periodic table for black hole orbits. *Physical Review D*, 77(10):103005, 2008.

- [15] Saskia Grunau and Valeria Kagramanova. Geodesics of electrically and magnetically charged test particles in the reissner-nordström space-time: Analytical solutions. *Physical Review D*, 83(4):044009, 2011.
- [16] Edward Belbruno and Frans Pretorius. A dynamical system's approach to schwarzschild null geodesics. *Classical and Quantum Gravity*, 28(19):195007, 2011.
- [17] Leor Barack and Norichika Sago. Beyond the geodesic approximation: Conservative effects of the gravitational self-force in eccentric orbits around a schwarzschild black hole. *Physical Review D*, 83(8):084023, 2011.
- [18] Daniela Pugliese, Hernando Quevedo, and Remo Ruffini. Circular motion of neutral test particles in reissner-nordström spacetime. *Physical Review D*, 83(2):024021, 2011.
- [19] Daniela Pugliese, Hernando Quevedo, and Remo Ruffini. Circular motion in reissner-nordström spacetime. In *The Twelfth Marcel Grossmann Meeting: On Recent Developments in Theoretical and Experimental General Relativity, Astrophysics and Relativistic Field Theories (In 3 Volumes)*, pages 1017–1021. World Scientific, 2012.
- [20] Kumar S. Virbhadra and George F. R. Ellis. Gravitational lensing by naked singularities. *Physical Review D*, 65(10):103004, 2002.
- [21] K. S. Virbhadra and C. R. Keeton. Time delay and magnification centroid due to gravitational lensing by black holes and naked singularities. *Physical Review D*, 77(12):124014, 2008.
- [22] Parthapratim Pradhan and Parthasarathi Majumdar. Circular orbits in extremal reissner-nordstrom spacetime. *Physics Letters A*, 375(3):474–479, 2011.
- [23] Marco Olivares, Joel Saavedra, Carlos Leiva, and José R. Villanueva. Motion of charged particles on the reissner-nordström (anti)-de sitter black hole spacetime. *Modern Physics Letters A*, 26(39):2923–2950, 2011.
- [24] J. R. Villanueva, Joel Saavedra, Marco Olivares, and Norman Cruz. Photons motion in charged anti-de sitter black holes. *Astrophysics and Space Science*, 344(2):437–446, 2013.
- [25] Daniela Pugliese, Hernando Quevedo, and Remo Ruffini. Motion of charged test particles in reissner-nordström spacetime. *Physical Review D*, 83(10):104052, 2011.
- [26] Daniela Pugliese, Hernando Quevedo, and Remo Ruffini. General classification of charged test particle circular orbits in reissner-nordström spacetime. *The European Physical Journal C*, 77(4):1–18, 2017.
- [27] Aleksandr Mikhailovich Lyapunov. The general problem of the stability of motion. *International Journal of Control*, 55(3):531–534, 1992.
- [28] Adilson E. Motter. Relativistic chaos is coordinate invariant. *Physical Review Letters*, 91(23):231101, 2003.
- [29] Jay Robert Dorfman. *An introduction to chaos in nonequilibrium statistical mechanics*. Number 14. Cambridge University Press, 1999.
- [30] V. Karas and D. Vokrouhlický. Chaotic motion of test particles in the ernst space-time. *General Relativity and Gravitation*, 24:729–743, 1992.
- [31] Neil J. Cornish and Janna Levin. Lyapunov timescales and black hole binaries. *Classical and Quantum Gravity*, 20(9):1649, 2003.
- [32] Frans Pretorius and Deepak Khurana. Black hole mergers and unstable circular orbits. *Classical and Quantum Gravity*, 24(12):S83, 2007.
- [33] Vitor Cardoso, Alex S. Miranda, Emanuele Berti, Helvi Witek, and Vilson T. Zanchin. Geodesic stability, lyapunov exponents, and quasinormal modes. *Physical Review D*, 79(6):064016, 2009.
- [34] M. R. Setare and D. Momeni. Geodesic stability for kehagias-sfetsos black hole in hořava-lifshitz gravity via lyapunov exponents. *International Journal of Theoretical Physics*, 50:106–113, 2011.
- [35] Sharmanthie Fernando. Schwarzschild black hole surrounded by quintessence: Null geodesics. *General Relativity and Gravitation*, 44:1857–1879, 2012.
- [36] B. Malakolkalami and K. Ghaderi. Schwarzschild-anti de sitter black hole with quintessence. *Astrophysics and Space Science*, 357(2):112, 2015.
- [37] Parthapratim Pradhan. Stability analysis and quasinormal modes of reissner-nordström space-time via lyapunov exponent. *Pramana*, 87:1–9, 2016.
- [38] K. Ghaderi. Geodesics of black holes with dark energy. *Astrophysics and Space Science*, 362(12):218, 2017.
- [39] Monimala Mondal, Parthapratim Pradhan, Farook Rahaman, and Indrani Karar. Geodesic stability and quasi normal modes via lyapunov exponent for hayward black hole. *Modern Physics Letters A*, 35(30):2050249, 2020.
- [40] Shobhit Giri and Hemwati Nandan. Stability analysis of geodesics and quasinormal modes of a dual stringy black hole via lyapunov exponents. *General Relativity and Gravitation*, 53(8):76, 2021.
- [41] Monimala Mondal, Farook Rahaman, and Ksh. Newton Singh. Lyapunov exponent, isco and kolmogorov-sinai entropy for kerr-kiselev black hole. *The European Physical Journal C*, 81:1–16, 2021.
- [42] Kourosh Nozari and Siamak Akhshabi. On the stability of planetary circular orbits in noncommutative spaces. *arXiv preprint gr-qc/0608076*, 2006.
- [43] Kourosh Nozari, Siamak Akhshabi, and Nasser Sadeghnezhad. Stability of circular orbits in noncommutative schwarzschild spacetime. *Acta Physica Polonica B*, 39(11), 2008.
- [44] Ravi Shankar Kuniyal, Rashmi Uniyal, Anindya Biswas, Hemwati Nandan, and K. D. Purohit. Null geodesics and red-blue shifts of photons emitted from geodesic particles around a noncommutative black hole space-time. *Modern Physics A*, 33(16):1850098, 2018.
- [45] Sehrish Iftikhar. Particle dynamics around a charged black hole. In *EPJ Web of Conferences*, volume 168, page 04006. EDP Sciences, 2018.
- [46] Alexis Larranaga. Geodesic structure of the noncommutative schwarzschild anti-de sitter black hole i: Timelike geodesics. *arXiv preprint arXiv:1110.0778*, 2011.

- [47] Piyali Bhar, Farook Rahaman, Ritabrata Biswas, and U. F. Mondal. Particles and scalar waves in noncommutative charged black hole spacetime. *Communications in Theoretical Physics*, 64(1):1, 2015.
- [48] F. Rahaman, I. Radinschi, U. F. Mondal, and P. Bhar. Particle's motion around a non-commutative black hole. *International Journal of Theoretical Physics*, 54(3):1038–1051, 2015.
- [49] M. A. Anacleto, F. A. Brito, B. R. Carvalho, and E. Passos. Noncommutative correction to the entropy of btz black hole with gup. *Advances in High Energy Physics*, 2021(1):6633684, 2021.
- [50] J. R. Nascimento, A. Yu. Petrov, P. J. Porfírio, Ali Övgün, and et al. Properties of an axisymmetric lorentzian non-commutative black hole. *arXiv preprint arXiv:2411.04674*, 2024.
- [51] J. R. Nascimento, A. Yu. Petrov, P. J. Porfírio, Ali Övgün, and et al. Effects of non-commutative geometry on black hole properties. *arXiv preprint arXiv:2406.12015*, 2024.
- [52] S. C. Ulhoa, R. G. G. Amorim, and A. F. Santos. On non-commutative geodesic motion. *General Relativity and Gravitation*, 46(7):1760, 2014.
- [53] Mohamed Aimen Larbi, Slimane Zaim, and Abdellah Touati. Geodesic motion of a test particle around a noncommutative schwarzschild anti-de sitter black hole. *arXiv preprint arXiv:2411.16886*, 2024.
- [54] Abdellah Touati and Slimane Zaim. Geodesic equation in non-commutative gauge theory of gravity. *Chinese Physics C*, 46(10):105101, 2022.
- [55] Abdellah Touati and Slimane Zaim. The bound of the non-commutative parameter based on gravitational measurements. In *Physical Sciences Forum*, volume 7, page 54. MDPI, 2023.
- [56] Narges Heidari, Hassan Hassanabadi, A. A. Araújo Filho, John Kriz, and et al. Exploring non-commutativity as a perturbation in the schwarzschild black hole: Quasinormal modes, scattering, and shadows. *The European Physical Journal C*, 84(6):566, 2024.
- [57] Yaqi Zhao, Yifu Cai, S. Das, G. Lambiase, E. N. Saridakis, and E. C. Vagenas. Quasinormal modes in noncommutative schwarzschild black holes. *Nuclear Physics B*, 1004:116545, 2024.
- [58] N. Heidari, H. Hassanabadi, A. A. Araújo Filho, J. Kriz, S. Zare, and P. J. Porfírio. Gravitational signatures of a non-commutative stable black hole. *Physics of the Dark Universe*, 43:101382, 2024.
- [59] N. Heidari, Ali Övgün, and et al. Quantum gravity effects on particle creation and evaporation in a non-commutative black hole via mass deformation. *arXiv preprint arXiv:2409.03566*, 2024.
- [60] N. Heidari, Ali Övgün, and et al. Geodesics, accretion disk, gravitational lensing, time delay, and effects on neutrinos induced by a non-commutative black hole. *arXiv preprint arXiv:2412.08369*, 2024.
- [61] Grigoris Panotopoulos and Ángel Rincón. Quasinormal modes of five-dimensional black holes in non-commutative geometry. *The European Physical Journal Plus*, 135(1):33, 2020.
- [62] Avijit Bera, Surojit Dalui, Subir Ghosh, and Elias C. Vagenas. Quantum corrections enhance chaos: Study of particle motion near a generalized schwarzschild black hole. *Physics Letters B*, 829:137033, 2022.
- [63] Shobhit Giri, Hemwati Nandan, Lokesh Kumar Joshi, and Sunil D. Maharaj. Geodesic stability and quasinormal modes of non-commutative schwarzschild black hole employing lyapunov exponent. *The European Physical Journal Plus*, 137(2):1–11, 2022.
- [64] Nathan Seiberg and Edward Witten. String theory and noncommutative geometry. *Journal of High Energy Physics*, 1999(09):032, 1999.
- [65] Xavier Calmet and Archil Kobakhidze. Second order noncommutative corrections to gravity. *Physical Review D*, 74(4):047702, 2006.
- [66] Paolo Aschieri and Leonardo Castellani. Noncommutative d= 4 gravity coupled to fermions. *Journal of High Energy Physics*, 2009(06):086, 2009.
- [67] Paolo Aschieri and Leonardo Castellani. Noncommutative gravity coupled to fermions: Second order expansion via seiberg-witten map. *Journal of High Energy Physics*, 2012(7):1–27, 2012.
- [68] Abdellah Touati and Slimane Zaim. On modified first law of black hole thermodynamics in the non-commutative gauge theory. *arXiv preprint arXiv:2205.13052*, 2022.
- [69] Abdellah Touati and Slimane Zaim. Thermodynamic properties of schwarzschild black hole in non-commutative gauge theory of gravity. *Annals of Physics*, 455:169394, 2023.
- [70] Ali H. Chamseddine. Deforming einstein's gravity. *Physics Letters B*, 504(1-2):33–37, 2001.
- [71] Masud Chaichian, Anca Tureanu, and G. Zet. Corrections to schwarzschild solution in noncommutative gauge theory of gravity. *Physics Letters B*, 660(5):573–578, 2008.
- [72] Zening Yan, Chen Wu, and Wenjun Guo. Scalar field quasinormal modes of noncommutative high dimensional schwarzschild-tangherlini black hole spacetime with smeared matter sources. *Nuclear Physics B*, 961:115217, 2020.
- [73] Javlon Rayimbaev, Ashfaque Hussain Bokhari, and Bobomurat Ahmedov. Quasiperiodic oscillations from noncommutative inspired black holes. *Classical and Quantum Gravity*, 39(7):075021, 2022.
- [74] Mohaddese Heydari-Fard, Malihe Heydari-Fard, and Hamid Reza Sepangi. Null geodesics and shadow of hairy black holes in einstein-maxwell-dilaton gravity. *Physical Review D*, 105(12):124009, 2022.
- [75] N. Heidari, H. Hassanabadi, J. Kuriuz, S. Zare, P. J. Porfírio, and et al. Gravitational signatures of a non-commutative stable black hole. *arXiv preprint arXiv:2305.06838*, 2023.
- [76] Majid Karimabadi, S. Aliasghar Alavi, and Davood Mahdavian Yekta. Non-commutative effects on gravitational measurements. *Classical and Quantum Gravity*, 37(8):085009, 2020.
- [77] The Event Horizon Telescope Collaboration and et al. First m87 event horizon telescope results. i. the shadow of the supermassive black hole. *The Astrophysical Journal Letters*, 875(1):L1, 2019.

- [78] Joby PK, Pravabati Chingangbam, and Subinoy Das. Constraint on noncommutative spacetime from planck data. *Physical Review D*, 91(8):083503, 2015.
- [79] B. Mirza and M. Dehghani. Noncommutative geometry and classical orbits of particles in a central force potential. *Communications in Theoretical Physics*, 42(2):183, 2004.
- [80] Juan M. Romero and J. David Vergara. The kepler problem and noncommutativity. *Modern Physics Letters A*, 18(24):1673–1680, 2003.